Microbial Potentiometric Sensor Monitoring of Milk Fermentation

by

Lucien Dieter

A Thesis Presented in Partial Fulfillment
of the Requirements for the Degree
Master of Science

Approved April 2022 by the
Graduate Supervisory Committee:

Kirl D. Hristovski, Chair
Larry W. Olson
Olcay Ünver

ARIZONA STATE UNIVERSITY

May 2022

ABSTRACT

Microbial Potentiometric Sensors (MPS) utilize endemic biofilms to generate a signal using a measurable potentiometric difference, without the use of cleaning, maintenance, and reagents of conventional sensor monitoring methods. These advantages are suitable for monitoring bioreactions in water distribution systems, soils, and wastewater treatment. In controlled fermentation processes, monitoring seeks to avoid contamination and degradation, which results in loss of productivity. MPS have yet to be applied to monitor the fermentation of milk to yogurt. This study examined the feasibility of using MPS technology to monitor the progress of milk fermentation in real-time with a bench-scale model bioreactor. Signal data obtained by the MPS was analyzed and assessed for the ability to model and predict the time of complete fermentation. Analysis of complete fermentation times in conjunction with pH and MPS signal values found characteristics indicative of complete fermentation. The method detection limit was assessed to inform of the method's capacity to distinguish complete fermentation time. A sensitivity analysis was conducted to develop a more robust method for predicting complete fermentation time. At this proof-of-concept scale, MPS successfully performed in this capacity to monitor bioreaction conditions continuously. MPS captured information as fermentation progressed, was completed, and as the yogurt product naturally began to decay. Analysis of the data obtained with the technology found predictions of complete fermentation time within a two hour range, with further assessment in the sensitivity analysis narrowing this timeframe to less than 45 minutes. This study revealed the challenges in precisely predicting complete fermentation;

however, advancement of a robust analytical method and demonstration of technical feasibility promotes further MPS technology applications that seek to monitor conditions in real-time to preserve health and production.

ACKNOWLEDGMENTS

As a student of ASU, I acknowledge that the Tempe campus sits on the ancestral homelands of those American Indian tribes that have inhabited this place for centuries, including the Akimel O'odham (Pima) and Pee Posh (Maricopa) peoples.

TABLE OF CONTENTS

Page

LIST OF TABLES..……...vii

LIST OF FIGURES……..viii

CHAPTER

1 INTRODUCTION……..1

Background and Hypothesis of the study……3

Research Objectives…….4

Assumptions and Limitations……..6

2 LITERATURE REVIEW…..……..8

Introduction of Data Applications……...8

Conventional Field Probes: Applications, Limitations, and Standard Expectations…….8

Common Water Quality and Environmental Parameters: Health-Based Regulatory Considerations……12

Public Health Impacts of Biofilm……..12

Formation of Biofilm: Elements and Factors of Attachment and Development……..……13

Biofilm Composition: Physical Accumulation in Water Environments…….16

Biofilm Self-Communication and Synchronization……...17

CHAPTER Page

MPS Technology: Principles, Development and Previous Advances, and Demonstrated Successes……...……18

Related Sensing Technologies: Electrochemical, Voltammetric, Potentiometric, and Bioactive Sensors…….....22

Data Analysis: Interpretation of Data via Assembly, Computation, Algorithms, and Machine Learning/Artificial Intelligence Methods……..…25

Current and Future Deployment for MPS and Sensor Technologies: Water Monitoring, Fermented Food Production, and Health Monitoring……..29

Microbial Fermentation Reactions and Yogurt Production…...…37

3 METHODOLOGY……..…..……..44

Experimental Design and Method…….44

Preparation and Assembly of Data for Primary Analysis……..47

Primary Analysis……51

Method Detection Limit Calculation……..56

Sensitivity Analysis……57

4 RESULTS…….……..…..……..62

Description of Open Circuit Potential and pH Trends……...62

Compared Results……..68

Method Detection Limit……72

Sensitivity Analysis……...74

CHAPTER Page

5 CONCLUSION....……..…..……..85

Research Advancement……..85

Reflections…….87

Recommendations……..90

Field Contributions…….……91

REFERENCES……..94

APPENDIX

A LITERATURE REVIEW METHOD…….115

LIST OF TABLES

Table Page

1. Complete Fermentaiton Data....70
2. Average Complete Fermentation Time Analysis....70
3. Calculation of the Method Detection Limit (MDL) 73
4. First Clustered Complete Fermentation Time Analysis- 2.041 g Inoculum Mass.76
5. Second Clustered Complete Fermentation Time Analysis- 2.0425 ± 0.0001 g Inoculum Mass. 77
6. Complete Fermentation Ranges 80
7. First Clustered Complete Fermentation Time Range Analysis- 2.041 g Inoculum Mass....82
8. Second Clustered Complete Fermentation Time Range Analysis- 2.0425 ± 0.0001 g Inoculum Mass 83
9. All Experiments Clustered Complete Fermentation Time Range Analysis- 2.042 ± 0.001 g Inoculum Mass 84

LIST OF FIGURES

Figure Page

1. Electrode Setup....45

2. Initial Experimental Test with 0.508 g Inocuulum Mass- Averaged MPS Signal and pH 63

3. Average MPS Signal and pH using 2.027 g Inoculum Mass....64

4. Average MPS Signal and pH using 2.041 g Inoculum Mass....65

5. Average MPS Signal and pH using 2.042 g Inoculum Mass....66

6. Average MPS Signal and pH using 2.041 g Inoculum Mass....67

7. Average MPS Signal and pH using 2.043 g Inoculum MassSignal and pH 68

8. Combined Experimental Data....69

9. Method Detection Limit (MDL) for Time....74

CHAPTER 1

INTRODUCTION

Microbial Potentiometric Sensors (MPS) utilize environmental microorganisms on the surface of graphite electrodes, generating a signal using measurable microbial potentiometric difference (Burge et al., 2020). MPS technology provides an ideal environmental or process monitoring tool by leveraging their simplicity and durability; operation without additional equipment, cleaning or maintenance; and lower cost of manufacture and operation in comparison to traditional monitoring methods (Wilson et al., 2019). A knowledge gap remains that limits the further advancement of potential MPS applications. Previous developments and similarly related studies provide relevant documentation to inform this research, including demonstrated parameters MPS can measure (Saboe et al., 2021), continual collection of real-time data (Burge et al., 2020), comparison of performance against traditional analytical instruments (Saboe et al., 2021b), and the development and processing of signal analysis to interpret data (Saboe et al., 2021a; Winquist et al., 1998).

With this detailed history of advancement, MPS and similar sensor technologies can advance further applications of electrochemical sensor technologies and approaches. Equipped with demonstrated ability of obtaining data, understanding the real-time state of an environment or monitored process allows for management to appropriately respond and safeguard health, production, and proper functioning of a process. Quantifiable multivariate information allows for the characterization and identification of a biological process using parameters including pH, oxidation-reduction potential (ORP), open-circuit

potential (OCP), dissolved oxygen (DO), turbidity and bioactivity (Burge et al., 2020; Favre et al., 2009; Holtmann et al., 2006). These parameters have been obtained using MPS technology in settings including water (Brown et al., 2020), soil (Burge et al., 2021), representative surface water (Saboe et al., 2021a), water distribution networks (Saboe et al., 2021b), and wastewater (Burge et al., 2020).

In this study, the fermentation of milk into a yogurt product served as a model fermentation process. Of the most direct relevance to this study, Winquist and colleagues explicitly suggest the paring of a similar electrochemical monitoring sensor in milk culturing while obtaining additional parameters (Winquist et al., 1998). The pH of a milk mixture has been measured using a similar voltametric method while culturing kefir (Casimero et al., 2018), a related fermented dairy product. Also of particular relevance, Ahari and coworkers as well as Favre and colleagues have experimented with electrochemical and microbial activity sensors in bacterial (Ahari et al., 2017) and fungi (Favre et al., 2009) applications, respectively. Chinnathambi and Euverink and further directly impose pH monitoring via a graphite sensor during the production of lactic acid from bacterial fermentation (Chinnathambi & Euverink, 2019).

In the expanding interest of microbial sensing technology and the monitoring this enables, additional capabilities of these sensors have yet to be tested. The results of testing new applications will advance their deployments into additional environmental settings to obtain and characterize environmental quality parameters and indicators. With the demonstrated detection capabilities in previous research, further study was designed to inform and assess sensitivities of MPS systems in additional media. This targeted study

tested the ability of the MPS to perform in a *L. acidophilus, L. bulgaricus,* and *S. thermophilus* produced yogurt culture of organic whole milk. By applying the same systematic tools of previous MPS technology, observing the produced signals in this new yogurt medium enables the assessment of the technology to perform in the same behavior as in previous mediums.

Goal and Hypothesis of the Study

The ability of MPS to determine microbial health indicators that are incongruent from predicted values or in greater resolution than those obtained by traditional sensing methods is sufficient for operational managers to identify health risks and take action. Traditional probes and sensors are limited, retrieving unreliable readings, requiring maintenance and cleaning, manual collection and potential laboratory processing, utilizing additional materials, recalibration procedures, and the potential to contaminate or consume a sample (Chinnathambi & Euverink, 2019). Delated data does not reflect current conditions (Chinnathambi & Euverink, 2019; Draz et al., 2021), limiting the usefulness of obtained information.

The real-time and continuous data collected by MPS provides operators with information of current conditions, allowing for adjustments to be made based on these observations. The lower cost and simple deployment of MPS in a variety of settings and situations is ideal to protect health and safety. Biofilm infections may be quickly realized before posing a threat to health (Jamal et al., 2018), including when contaminating food products (Draz et al., 2021). Equipped with MPS data, considerations of health and

safety, productivity, processing conditions and controls, and optimal management are more readily made using the real-time information.

To evaluate the performance of MPS in the yogurt fermentation process, the goal of this study was to test the ability of MPS to monitor the temporal changes in open-circuit potential during the yogurt fermentation process. Behind this goal, the underlying hypothesis was that the yogurt fermentation could be monitored by temporal change in open-circuit potential by microorganisms at different stages of the fermentation process. The sensitivity of the MPS technology was selected so as to predict with 95% confidence the time at which fermentation is completed. By selecting the 95% confidence, a precision assessment was performed to answer the research question and assess whether the MPS technology could be used to determine the time of complete yogurt fermentation.

Research Objectives

To address the goal of this study, four research objectives were established. First, a systematic literature review was performed to assist the design of a targeted experimental setup investigating the relationship between biological activity and MPS signal generation. The process and method of obtaining the literature is outlined in Appendix A. The targeted relationship was examined with MPS which was used to characterize a profile of MPS signal and pH over time. For this signal analysis to be performed, the second research objective was to obtain these quantifiable data targets, including MPS signal and pH. From here, the third research objective analyzed

representative signals with pH to determine indicators of fermentation completion. Signal analysis formed the primary result analysis of this research. The fermentation process was considered complete when the experimental mixture's pH stabilized around pH = 4.6 (de Oliveira, 2014), which was simultaneously identified using MPS signals.

At last, the fourth research objective was to analyze the sensitivity of the MPS technology by calculating a method detection limit (MDL). The MDL informs the analytical method's precision and confidence in determining the minimal amount of time the calculation may report (U.S. EPA, Office of Water, 2016). The fourth research objective includes the sensitivity analysis (Thabane et al., 2013), accounting for and adjusting different metrics produced from the experimental trials to examine if statistically significantly different results occur from alterations in the experimental method, data computation, and modeling to support the robustness of the obtained results. The same data used in the primary analysis of the third research objective yet through different analytical methods in this sensitivity analysis was compared. The effect of changing the analytical method in this sensitivity analysis serves to determine the most robust method of analysis and the confidence of the results. The sensitivity analysis may examine the effects on results when definitions are slightly changed, such as complete fermentation time cut-offs, inclusion or exclusion of outlier trials, or the grouping of similar experimental trial clusters (Thabane et al., 2010). Combined with the MDL, the feasibility of using MPS technology and the paring with the most robust analytical method to determine complete fermentation may at last be determined.

Assumptions and Limitations

This research was limited in scope and abilities to a bench-scale experiment. It was a known limitation that redox potentials are unreliable without constant, standard equilibrium conditions (Burge et al., 2020) that would only be found under precisely controlled experimental settings. However, this is the case of true-to-life environmental conditions of which this technology is suggested to be utilized. Environmental biofilms are variable and always in flow (Thomen et al., 2017), not in a static and clinical condition. Commercial manufacture of yogurt is a carefully controlled process, with temperature a determining parameter of the final product's characteristics, stable shelf life, and health and safety (de Oliveira, 2014). While effort was made to control the temperature of the reaction in this study within ± 1 ºC, it was assumed that the study occurred under approximately constant temperature. Temperature was recorded as an additional parameter. However, in face of potential temperature fluctuations, a 10 ºC optimal temperature range (Ahari et al., 2017) provides an adequate margin for this study to capture this microbial process. Additionally, the method used to culture the model yogurt in this study was assumed to be completely mixed. While effort was made to ensure homogenous distribution of the lyophilized inoculating culture blend at the start of each experiment, the mixture was not continually stirred. In turn, this resembles the process for the production of set yogurt, where yogurt obtains the characteristic gel structure by fermenting the starting milk within the final product vessel (de Oliveira, 2014). This is in contrast to another yogurt production method, stirred yogurt, where the

mixture is stirred and this gel structure is broken, repackaged, and allowed to solidify again following fermentation (de Oliveira, 2014).

While this study utilizes bacteria that is adapted for growth in milk at moderate temperatures (de Oliveira, 2014), it is also estimated that 95% of all microorganism form biofilm structures (Flemming et al., 2002), the biological component that enables the functionality of MPS in any environment. With these assumptions known, they may in turn play a role in the results of the experimental trials; as such, the sensitivity analysis will examine and document different outcomes that result from approaching the research and these assumptions differently.

CHAPTER 2

LITERATURE REVIEW

Introduction of Data Applications

Acquisition and control of data has the power to significantly improve wastewater treatment plant operations and management (Pereira et al., 2019). In advancing analytical methods to monitor real-time processes, expenses should be reduced and long-term reliability assured (Hall & Szabo, 2009; Jiang et al., 2019; Shao et al., 2020; Stoianov et al., 2008; U.S. EPA, 2015). The role of biofilms in the onset of infection suggests the need to advance early detection technologies (Poma et al., 2020). The real-time reporting offered by MPS allows management to be equipped with data that can predict incoming changes (Burge et al., 2020). Monitoring of food safety control to maintain food quality drives development of such sensors (Draz et al., 2021). Detection of biofilm should combine high sensitivity, rapid response time, low cost, and the ability for miniaturization- all of which are achieved by MPS.

Conventional Field Probes: Applications, Limitations, and Standard Expectations

Field probes are used to capture a measurement or environmental characteristic, often requiring laboratory processing before a final result can be produced. Typical monitoring systems use data collected from sensors and probes that measure dissolved oxygen, pH, and oxidation-reduction potential (Burge et al., 2020). These probes are subject to regular maintenance, recalibration, and replacement (T. Nguyen et al., 2012),

as well as cleaning to remove accumulated biofilm and sediments (Blaen et al., 2016; Meyer et al., 2019; Wiranto et al., 2015).

Probes that measure physicochemical parameters are limited by the interdependence of electrochemical potential and pH (Bohrerova et al., 2004; Dowley et al., 1998; Hinsinger et al., 2006; Husson, 2013; Liptzin et al., 2011; Mansfeldt, 2003; Mueller et al., 2001; Rabenhorst et al., 2009; Rice et al., 2018; Sophocleous & Atkinson, 2017; Wanzek et al., 2018). U.S. regulations mandate continuous and real-time monitoring of residual free chlorine at the point of water discharge (40 CFR § 141.74 - Analytical and Monitoring Requirements). However, monitoring is often practiced manually. The lack of reliable chlorine sensors that are appropriate for long-term monitoring in drinking water distribution systems poses a challenge to continuous and real-time monitoring (Wilson et al., 2019). In batch-driven processes, discharges of exotoxins may be characterized in pulses, a challenge to operators to monitor and control processing. Monitoring is typically dependent on intermittent grab sampling followed by laboratory analysis, which does not characterize the profile of an operation's composition due to low sampling frequency and irregular discharges (Brown et al., 2020). Accurate monitoring of the composition of a process and its contents allows for greater regulatory and enforcement power to prevent undesired releases.

There is often a disparity between supposed and actual chlorine residuals, with measured levels lower than predicted due to low demand in dead-end distribution points and extremities of supply systems (Abokifa et al., 2016). Biofilm growth proliferates as inadequate free chlorine residuals are coupled with high disinfection biproducts.

Further, traditional sensors read erratic measurements as the detection and quantification limits are strained, loosing accuracy and precision at low observation levels (Saboe, et al., 2021a). Traditional glass pH probes are often incompatible with miniaturized and biomedical systems (Casimero et al., 2018). Traditional pH electrode probes of this variety are glass-based and fragile, relatively large, and may leak an electrolyte solution into a sample (Chinnathambi & Euverink, 2019). An advantage of alternative pH measurement would allow for site-specific application and measurement at the electrode, despite the shape or size of deployment. Alternative pH electrodes may be deployed in environments where the diffusion of traditional sensor solutions is to be avoided, such as in food and health processes, as the electrode does not contain internal solutions that can diffuse into a sample (Chinnathambi & Euverink, 2019). Rapid and direct determination of the content in a food product using a potentiometric method, in contrast to chromatographic or other traditional methods, is simple as it saves chemicals, solvents, time and resources, and produces fewer wastes (Draz et al., 2021).

Microbial detection techniques including culture-based and molecular-based methods provide information about the nature of the biofilm, yet are not suitable for real-time monitoring (Azeredo et al., 2017). Culture-based approaches combined with molecular DNA methods are used to identify and quantify microorganisms within biofilms (Wi & Patel, 2018). Despite this identification, these methods are affected by low sensitivity and do not allow for the real-time monitoring of biofilms (Hall-Stoodley et al., 2012). Culture-based techniques rely on the growth of viable microorganisms in a culture media. However, not all microorganisms are able to grow on laboratory media

(Nivens et al., 2009). Further, some microorganisms embedded in biofilms are present in different physiological states, so they may be viable but not-culturable (VBNC) (Azeredo et al., 2017). Molecular methods of detecting biofilm DNA are not informative about the viability of detected microorganisms, as positive detections may be from extracellular or non-viable elements (Hall-Stoodley et al., 2012).

Microscopy is the most common technique to characterize biofilm structure (Azeredo et al., 2017; Lewandowski & Beyenal, 2013). Electron microscopy techniques, including transmission electron microscopy and scanning electron microscopy, produce a higher resolution of microbial cell imaging and the surrounding environment (Poma et al., 2021). Both of these microscopy techniques, however, do not allow for *in vivo* and *in situ* measurements as they are vacuum techniques, requiring extensive sample treatment that may damage the biofilm's structure (Surman et al., 1996). As a result, these approaches are not appropriate for the sensing desires of this research.

Previous potentiometric reference electrodes, composed of silver- silver-chloride, glass, or platinum require an internal electrolyte solution (Burge et al., 2020; Vonau et al., 2010). When this electrode is placed in an environmental medium, such as dry soil, the solution is lost, preventing many reference electrodes from being deployed in additional mediums (Fiedler et al., 2007). In comparison, graphite MPS performs with greater long-term consistency and invariability of patterns (Burge et al., 2021).

Common Water Quality and Environmental Parameters: Health-Based Regulatory Considerations

Collection of data is required for regulatory compliance; however, due to manual sampling and subsequent laboratory processing, data is discrete and often insufficient to address real-time operation and management (Spellman, 2003; Trussell et al., 2007). Chlorination is the dominant disinfectant for drinking water, used by over 80% of public water utilities (U.S. EPA, Office of Water, 1999). Residual chlorine in pipelines prevents the expansion of microorganisms through storage and distribution. Residual free chlorine is low cost and serves to protect drinking water quality through to distribution (American Chlorine Chemistry Council, 2003). Monitoring and control of pH is an important parameter in regard to its effects to biochemical processes (Chinnathambi & Euverink, 2019).

Public Health Impacts of Biofilm

Biofilm growth presents a threat to public health. Biofilms are responsible for approximately 80% of human microbial infections in the medical field (Jamal et al., 2018; Khatoon et al., 2018). An estimated 8% of water utilities in the United States report health-based standard violations (Allaire et al., 2018), which are frequently attributed to excessive total coliforms and disinfection byproducts.

Culture-based diagnosis is time-consuming, requires specialized personnel, and cannot monitor biofilm in real-time (Hall-Stoodley et al., 2012). This presents a need for real-time monitoring and *in situ* biofilm detection (Vertes et al., 2012).

Monitoring for food safety quality is designed to safeguard consumer health and maintain food industry welfare. Chemical and biological hazards result from contamination of food products, as well as adulteration, mishandling, and improper storage (Draz et al., 2021). Analytical methods should provide accurate and reliable information in a cost-effective and timely manner. This information is then referenced by authorities when making decisions (FAO, 2018).

Quality control of food products may be assessed by microbial diagnosis. The presence of exotoxins can be determined by measuring electrode potential (Ahari et al., 2017). In quality control tests, the ability of biosensors to detect exotoxins can assist research and health, yet are affected by temperature and acidity (Ahari et al., 2017). This directly informs this research to monitor pH and temperature in tandem to MPS signal. Bacterial detection speed increases as the size of the nanoparticle decreases (Tang et al., 2008).

The demonstrated ability of a MPS to determine critical microbial health indicators that are incongruent from predicted levels or those obtained by traditional sensing techniques is sufficient for operators to identify health risks and take action. The lower cost and simple deployment of MPS is ideal for systems to readily protect human health.

Formation of Biofilm: Elements and Factors of Attachment and Development

Establishment of biofilms in water distribution systems can advance on freshly cleaned pipelines within two weeks, even with residual chlorine present (Fish & Boxall,

2018). Once established, biofilms are difficult to remove, as even chlorine concentrations above the maximum targeted 4 mg/L cannot eradicate the biofilm, further accelerating the formation of carcinogenic disinfection biproducts (X. Bai et al., 2015; LeChevallier et al., 1990). Biofilm develops in two distinct phases: first, a reversible and irreversible attachment to a surface, followed by the formation of microcolonies, before the biofilm matures and disperses (Monds & O'Toole, 2009).

The initial attachment of microorganisms to abiotic surfaces is dependent on the properties of the material and the microbial cell surface (Poma et al., 2021). This is generally mediated by non-specific phenomena, including hydrophobic, electrostatic, steric interactions, and van der Waals forces (Dunne, 2002). Colony growth begins irreversibly following the accumulation of an initial layer of cell clusters called microcolonies. During biofilm maturation, microorganisms actively proliferate (Dunne, 2002). Molecules, enzymes and nutrients accumulate as biofilms form complex three-dimensional structures populated by different microenvironments and different metabolic activities (Stewart & Franklin, 2008). As the biofilm disperses, cells and cell clusters spread to new locations (Kaplan, 2010), which may be in response to environmental condition changes including the accumulation of metabolites, depletion of nutrients or oxygen (McDougald et al., 2012).

The formation of biofilm is typically irreversible; once established, the biofilm cannot be easily removed (Poma et al., 2020). As such, the formation of biofilm may be detrimental to public health and the productivity of an industry (Macià et al., 2018; Mattila-Sandholm & Wirtanen, 1992). In industry, contamination with pathogenetic

organisms leads to poor end-product quality (Mattila-Sandholm & Wirtanen, 1992; Telegdi et al., 2017). This presents the need for on-site detection and real-time monitoring of biofilm formation to promptly help direct operational measures.

Body tissues infected by biofilms or medical devices infected with biofilm may be required to be removed (Wu et al., 2015), highlighting the irreversible severity of biofilm infections. Bacterial infections from *Staphylococcus epidermidis, S. aureus, Pseudomonas aeruginosa* and *Escherichia coli* are most common (Mermel, 2000). The occurrence of infection is dependent on these microorganisms, substrate characteristics, and nutrient availability (Donlan, 2001; Jamal et al., 2018).

An estimated 95% of all microorganisms affix to the inner surfaces of pipes and vessels as biofilms (Flemming et al., 2002). These walls offer refuges that protect the biofilm from disinfection agents. Biofilms may grow in areas that are challenging to access, such as water pipes (Hall-Stoodley et al., 2012). The ability of biofilms to form on many substrates in many environment poses them to be a serious threat to health and industrial productivity (Poma et al., 2021). Several systems advanced thus far may monitor the growth of biofilms, however the future development of MPS sensors and applicable deployment settings have yet to be fully realized. MPS utilize the ubiquitous survival capabilities of existing environmental biofilms, allowing for increased efficacy of antimicrobial operations and advance control measures to be informed.

Biofilm Composition: Physical Accumulation in Water Environments

Biofilms are complex and dynamic structures, heterogeneous as a result of interactions of nutrient availability, varying surface topography, sheer stress, microbial species, and metabolism (Flemming et al., 2016; Lopez et al., 2010). Biofilms are stratified into layers, with anabolic activity decreasing as the distance from an electrode increases (Chadwick et al., 2019). The structural, chemical, and physiological characteristics of biofilm are subject to minute adjustments in pH which may alter a biochemical process, adversely affecting the outcome (Chinnathambi & Euverink, 2019).

Most toxic metals interfere with biochemical processes that impact the functioning of both microbial and multicellular organisms (Zeng et al., 2020). Toxic metal pollutants harm proper biological conditions and disrupt the proper functioning of water treatment processes (Bhat et al., 2020; Kumar et al., 2020). Toxic metals are presumed to therefore decrease metabolic activity of biofilm microorganisms, including the microbes populating the surface of a MPS (Brown et al., 2020). The change in open-circuit potential generated by the biofilm could be associated with microbial activity on the sensor, linking toxic metal effects on environmental microbes to a measurable microbial potentiometric difference.

Microbial respiration using extracellular substrates may be harnessed for technologies including water desalination (Brastad & He, 2013; Schievano et al., 2016), wastewater treatment (Logan & Rabaey, 2012), and of most interest to this research, fermentation, (Moscoviz et al., 2016; Schievano et al., 2016). The streamlining of extracellular electron transfer accelerates the per-cell respiration rate, altering the biofilm

structure to improve the efficiency of electron transfer (Jiménez Otero et al., 2021). As biofilms are typically diverse microbial structures; a MPS does not have to be selective, rather the lack of sensitivity is advantageous in applications where microbial composition may change (Poma et al., 2020).

Biofilm Self-Communication and Synchronization

Biofilms have the ability to communicate metabolism via electrochemical signaling. This is achieved as the production of ammonium is directed by electrochemical signaling, where inner and peripheral biofilm membrane potentials oscillate as potassium ion gradients shift (Saboe, et al., 2021b). Bacterial ion channels propagate these potassium ion waves, which in turn triggers the release of intracellular potassium that then depolarizes adjacent cells (Prindle et al., 2015). The function of this ability distributes nutrients across the biofilm as needed for growth, achieved by synchronizing the biofilm's resting membrane potential (Liu et al., 2015). This allows bacterial cells to rapidly communicate their metabolic state across relatively long distances. The oscillation of this ion diffusion enables biofilms to synchronize and coordinate their metabolism by exchanging the potassium ions between the inner and outer biofilm layers (Prindle et al., 2015). This symbiotic relationship of the microbial communities that compose biofilms provides the hardiness of biofilms (LeChevallier et al., 1990).

The electrochemical potential of biofilms is akin to a transmembrane potential; the metabolic state of both the individual cells and biofilm composite defines a voltage potential. At the microorganism community size, biofilm-coated electrodes have

measured positive linear trends in capacitance and negative linear trends in open circuit potential (Bimakr et al., 2018). This has been confirmed by previous studies; pH has been demonstrated to shape cell activity within biofilm (Franks et al., 2009; Logan, 2009; Torres et al., 2008), and electrical potential dependencies similarly shape cell activity (Levar et al., 2014; Li et al., 2019; Rimboud et al., 2015; Snider et al., 2012; Yoho et al., 2014, 2015; Zacharoff et al., 2016). Only recently was a robust and direct method used to obtain spatially resolved cell data (He et al., 2021). This method finds that the first 5 μm of a biofilm that is closest to an electrode contributes between 61% and 79% of the total current density at high or low anode potential, respectively (He et al., 2021). Further, 83% and 98% of the current is produced within 10 μm of the anode and between 98% through 100% is produced from within 15 μm of the anode (He et al., 2021).

MPS Technology: Principles, Development and Previous Advances, and Demonstrated Successes

Potentiometry is an electrochemical technique that measures the open-circuit potential between a working electrode and a reference electrode when there is no current flowing (Bagotsky, 2005). Devices that measure this potential to monitor biofilm continue to be developed (Janknecht & Melo, 2003; Nivens et al., 1995).

As environmental biofilm regenerates on the surface of a MPS (Hyde, 2019; Rice et al., 2018), limitations typically associated with sensing probes are avoided. These limitations include changes in oxygen or nitrogen content (Whisler et al., 1974), high temporal variability within small horizontal distances (Fiedler, 2000), and attributions of

irreversible redox reactions, slow reaction kinetics, and mixed redox process potentials (Fiedler et al., 2007). Using endemic microbial biofilms as the active surface of non-oxidizable material enables the measurement of electrochemical potential (Burge et al., 2021). This enables the continual deployment of the sensor in the environment as the endemic microorganisms self-replicate on the sensing surface of the MPS (Hyde, 2019). The potentiometric measurements of MPS technology uses an indicator electrode, a reference electrode, and a high-impedance measurement circuit system to measure the open circuit potential of the electrodes (Burge et al., 2019). This allows the relation of pH and oxidation-reduction potential with solid state electrodes that measure the potential difference between the sensing and reference electrodes (Burge et al., 2020).

When the MPS electrodes are coated in biofilm, capacitance and open circuit potential from microbial electrochemical signaling can be measured (Bimakr et al., 2018; Xu et al., 2010). Biofilm is capable of detecting minute changes in the aquatic environment, responding with an associated open circuit potential, measured with a reference electrode (Saboe, et al., 2021a). As measurements are collected using the electric potential of an open circuit in which electrons are not flowing, sensor arrays may be referenced against a single reference electrode (Burge et al., 2020). The growth of biofilm on an electrode surface alters the electrochemical properties: charge transfer resistance decreases, which can occur with direct electron transfer from nanowires of cytochromes to the surface of the electrode (Xu et al., 2010). This sensing ability has been applied to measure many characteristics: the accumulation of biomass and contaminants in aquatic environments (Bimakr et al., 2018); pH (Ahari et al., 2017;

Burge et al., 2021; Chinnathambi & Euverink, 2019; Saboe et al., 2021a); oxidation-reduction potential (Brown et al., 2020; Burge et al., 2020, 2021); free residual chlorine in water (Brown et al., 2020; Burge et al., 2020; Saboe, et al., 2021a); blue-green algae, turbidity, and chlorophyll (Saboe et al., 2021a); toxic metals (Brown et al., 2020; Di Natale et al., 1997); and conductivity of water and soil (Burge et al., 2021; Favre et al., 2009; Saboe et al., 2021a). This multimetric sensing capability of MPS monitoring relieves the need for several probes, manual grab sampling, and dilatory laboratory analysis. The multivariate electrochemical parameters may be monitored continuously and in real time, such as the conductivity of water and soil matrices (Burge et al., 2021; Favre et al., 2009). Further, MPS do not consume a sample itself (Chinnathambi & Euverink, 2019), preserving the original sample from being lost. MPS also avoid the additional equipment, biofoul cleaning, maintenance, and higher per unit costs of existing sensors (Wilson et al., 2019).

Electrodes exposed to biofilms therefore have the potential to monitor biomass accumulation and contaminants in an environmental matrix. The coating of biofilm over graphite electrodes can thus be combined with a reference electrode to form microbial potentiometric sensors, capable of measuring open circuit potential generated by biofilm (Brown et al., 2020; Burge et al., 2020; Saboe et al., 2021b). Logging continuous and real-time data of oxidation-reduction processes monitored by MPS can then be correlated to biofilm activity (Saboe et al., 2021b). As the microbial composition of biofilms is dynamic, responses to contaminants, nutrients, and temperature can be closely observed

by MPS, used to characterize biofilm over time rather than representing a single capture as traditional grab sampling would yield.

When operating in an open-circuit mode, microbial activity does not cease. Metabolically generated electrons flow to electron acceptors, however the open-circuit does not transport electrons to an acceptor near the cathode. As such, the transport of electrons from anode to cathode is interrupted. A more accurate description of this open-circuit mode is with the anode serving as a sensing electrode and the cathode as the reference electrode. The pair of electrodes cannot be used to create a signal based on electrical current flow, however the electrons generated from substrate metabolism can be stored in temporary electron acceptors (Magnuson et al., 2001; Myers & Myers, 2001). Electrons generated from organic carbon metabolism, for example, may be stored in cytochromes within the biofilm, especially in the absence of oxygen or nitrate as an electron acceptor (Bonanni et al., 2012; Esteve-Núñez et al., 2008; Rabaey et al., 2007; Schrott et al., 2011; Shi et al., 2007). The generation and storage of electrons in the biofilm creates a difference in open-circuit potential that may be measured between the sensing and reference electrodes. This is achieved as differential voltage increased when the concentration of dissolved organic compounds increases near the electrode, and similarly, when reducing concentrations of dissolved organic compounds in the constant presence of oxygen result in a falling differential voltage.

In water, microbial response signals have been seen to take over one month to develop and stabilize on the surface of the MPS sensor electrodes (Saboe, et al., 2021a). In soils, the deployment of MPS is limited by the quality and reliability of the

technology, which results in limited reliability of measurements (Burge et al., 2021). However, an experiment using MPS measurements found statistically different patterns in open circuit potential, suggesting that the conductivity and open circuit potential of soil is independent of water and carbon content (Burge et al., 2021). This primes the MPS technology to be deployed in a setting where these components would otherwise be dynamic and potentially interfere with other sensing methods.

In any sensing environment, factors including nutrients, temperature, and exotoxins can impact reaction kinetics and thus impact the differential voltages of sensing technology (Burge et al., 2020). It is anticipated that the growth of microbes that generate cytochromes will proliferate within the MPS biofilm, which readily responds to environmental fluctuations, making this sensor ideal for measuring changes in redox conditions. The biofilm surface serves as the active site of the sensor and also can regenerate (Rice et al., 2018), eliminating the requirement of routine cleaning and maintenance. Signals from MPS have been demonstrated to not decay over a two-year duration of deployment with no maintenance performed (Burge et al., 2020), demonstrating the long-term durability and reliability of the sensors.

Related Sensing Technologies: Electrochemical, Voltammetric, Potentiometric, and Bioactive Sensors

Electrochemical sensors are a method of detecting and monitoring biofilms. These sensors typically consist of an electrochemical cell with three electrodes: a working electrode, a reference electrode, and the counter electrode. These are immersed in an

electrolyte solution (Bagotsky, 2005; A. J. Bard & Faulkner, 2001; 1948- Wang Joseph, 2006). The sensing reaction occurs at the working electrode, which is typically constructed of platinum or gold (L. R. Bard & Faulkner, 2001). Electrochemical sensors provide a short response time, are low-cost, have high sensitivity, and are scalable (Thet et al., 2016). The low manufacturing costs of an electrode allow for the application of the technology where many pH electrodes are necessary, illustrating the scalability of this technology (Chinnathambi & Euverink, 2019).

Biofilm monitoring devices are currently focused on the application to water distribution systems (Strathmann et al., 2013). However, in most settings, oxidation-reduction potentials are unreliable without constant equilibrium conditions (Burge et al., 2020). In contrast, biofilm development is typically subjected to variable flow conditions, which is known to control and favor microbial adhesion, and may also serve as an environmental signal to influence biofouling (Manuel et al., 2007; Thomen et al., 2017; Weaver et al., 2012). The optimum pH range where potentials have been observed to remain significantly constant are between 5.0 and 8.5, with optimum temperatures between 15 ºC and 25 ºC (Ahari et al., 2017).

Voltammetric approaches of indirectly determining pH offers greater selectivity and faster response in comparison of conventional potentiometric sensors (Lafitte et al., 2008; Streeter et al., 2004). This approach measures current as a function of applied potential to an electrochemical cell, which is then plotted on a voltammogram (A. J. Bard & Faulkner, 2001; Eggins, 2002; Vivaldi et al., 2020). Voltammetric peaks are generated from the occurrence of electrochemical reactions at the working electrode (Scholz, 2015).

Voltammetry has been used to detect bacterial colonization on a surface as detected by a change in the electroreactive area (J. Kang et al., 2012). As a result, voltommetry may help to characterize the surface modifications of biofilm by evaluating the electroactive area, the presence of electroactive species at the working electrode, or the exchange of electrons between the biofilm and the electrode (Poma et al., 2021).

Redox reactions generate electrons that are used by cellular mediators, such as NADPH (Favre et al., 2009). Electrons can be transferred to extracellular surfaces after electrons cross through the cell membrane. This process occurs during anaerobic respiration (Bond & Lovley, 2003). Using this electron mechanism, electrochemical detection allows for the observation of microbial activity. Such activity is utilized in biological oxygen demand (BOD) sensors, where the reduction of oxygen is recorded by the anode (K. H. Kang et al., 2003). Similar sensors are used by wastewater treatment and can operate without maintenance for at least five years (Kim et al., 2003).

All bioactivity sensors allow for the measurement of microbial activity by recording potentiometric signals from aerobic and anerobic fermentation of glucose (Holtmann et al., 2006). Potentiometric sensors that detect and characterize biofilm are advantageous as they do not need an external power source (Poma et al., 2020). The open-circuit potential is measured between a working and reference electrode to assess the analyte's concentration and activity (Janknecht & Melo, 2003; Nivens et al., 1995). A change in the open-circuit potential may be associated to the biomass of biofilm (Gümpel et al., 2006; Mattila et al., 1997). Potentiometric sensors have also monitored pH gradients within a biofilm (Guimerà et al., 2019).

Data Analysis: Interpretation of Data via Assembly, Computation, Algorithms, and Machine Learning/Artificial Intelligence Methods

When MPS sensor data is collected, electrical current is not flowing, leaving the biofilm undisturbed. This allows for the direct observation of the biofilm (Burge et al., 2020). At the same time, measurement does not draw current from the sensors, which enables large arrays of sensors to be referenced against a single reference electrode. In development, an increasing concentration of oxygen measured by the dissolved oxygen probe and an increase in oxidation-reduction potential signal was paralleled by the data acquired by the MPS (Burge et al., 2020). An extremely low *p* value suggests a statistically strong and significant correlation between dissolved oxygen concentrations and the MPS signals. A pattern may be determined when compared to baseline signals, revealing information relevant for optimization of any process or condition where microbes are present.

The complexity of different water quality parameters interacting cannot be described using simple mathematical relationships, however machine learning tools can be trained to interpret these relationships. Continuous data collected with MPS technology can be disaggregated via machine learning, artificial intelligence, and software algorithms (Di Natale et al., 1997; Saboe et al., 2021a; Syafrudin et al., 2018; Winquist et al., 1998). Machine learning and artificial intelligence may optimize water quality management as data is collected and predicting additional parameters in real time (Syafrudin et al., 2018). While first needing sufficient data to train these tools, supplying data to these methods generates predictive power of a model, leveraging extrapolated

patterns from collected measurement. This is useful for environmental management to anticipate dynamic conditions and implement operational measures in real time (Pereira et al., 2019; Spellman, 2003; Trussell et al., 2007), providing advance anticipation of infections, exotoxins, or algal blooms with adequate time to apply operational measures. For example, data may be used to monitor metabolic activity in real time (Burge et al., 2020; Chinnathambi & Euverink, 2019; Favre et al., 2009). Early investigations monitoring microbial metabolic activity have deployed this capability during anaerobic respiration and fermentation (Ahari et al., 2017; Chinnathambi & Euverink, 2019; Favre et al., 2009; Holtmann et al., 2006; Winquist et al., 1998). An electronic sensor array, combined with a pattern-recognizing algorithm, has been used to measure metal ions in surface water (Di Natale et al., 1997). Here, working and reference electrodes were applied to a voltage, generating data that contains a large amount of information that may be interpreted by multivariate calibration methods. With this voltametric method, the multivariate analysis searches for a structure in the data which then is correlated to the data using a model (Winquist et al., 1998). Data is compared to a set of calibration data, and when combined, yield the model's predictive power. The measured data series contained high resolution, and despite many redundant values and an unknown detection limit of the sensor, this does not pose an issue at this concentration of bacterial content (Winquist et al., 1998).

A specific artificial intelligence approach, long short-term memory, has been used in a previous study to train machine learning tools (Saboe et al., 2021a). This neural network enables the tracking of long time-series data (Sak et al., 2014), which is suitable

for forecasting a series as desired for this application of MPS technology. This approach revealed a unique pattern of MPS data collected from water containing blue-green algae, illustrating a day and night cycle attributed to algae's exposure to sunlight. The synthesis of carbonaceous nutrients in algae requires electron transfer to a final electron donating oxygen, and at night in absence of sunlight, algae utilizes synthetic nutrients rather than carbon nutrients (Cuhel et al., 1984). The ability of machine learning and artificial intelligence to recognize this from the collected data and thus predict the concentration of blue-green algae with a high degree of precision demonstrates the function of this data analysis approach.

A relationship between open circuit potential and MPS signal output can be determined by assessing these patterns. Significant amounts of information can be leveraged from the analysis of the open circuit potential and signal patterns. Open circuit potential has been indicated to be directly resultant from reductions in microbial density and vitality, evidenced by the homogenous oxidation of biofilm on MPS and the elimination of electrons contained in cellular membranes (Saboe et al., 2021b). Another benefit of modeling results in a smaller error than that of commercially available amperometric sensors (Hach, 2018; Sensorx, 2011). In tandem with a smaller error, machine learning and artificial intelligence processing of MPS collected data is capable of predicting parameters below the level of readability of traditional analytical sensors (Saboe et al., 2021a). Deviations in data between MPS and traditional probes illustrates the capability of a MPS system to oversee the performance and detect the potential failures of other analytical equipment.

Assembling multiple arrays of MPS enables increased precision or predictive power. Connections of sensors to a wireless electronic circuit allows for further applications using wireless sensing (Azzarelli et al., 2014; Gou et al., 2015). At the same time, this constructs a multidimensional spatial characterization of a monitored environment (Saboe et al., 2021a). In soils, the assembly of an array of multiple sensors connected to a single reference electrode allows data generated to characterize both two-dimensional and three-dimensional unsaturated soil qualities (Burge et al., 2021). Deployment of sensors at multiple spatial and temporal settings allows the sensor array to document accurate data and support field usage to resolve thermodynamic conditions and dynamic metabolic processes (Burge et al., 2020). This capability may be then applied beyond water and soil; approaches in biomedical, agricultural, and climate research are associated to this MPS technology approach that characterizes various environmental fluctuations.

While this research will not employ comparable machine learning or artificial intelligence tools, this review illustrates the capacity for these tools to be paired with sensing and monitoring technologies. With the rich data produced by MPS technology and similar sensors, advanced computational approaches including machine learning and artificial intelligence will be equipped with burgeoning data to analyze and further refine the capabilities of producing extrapolated data from these sensing systems. As a result, combining MPS technology with these advanced approaches brings greater predictive power and informative depictions of the sensing environment.

Current and Future Deployment for MPS and Sensing Technologies: Water Monitoring, Fermented Food Production, and Health Monitoring

Biofilm monitoring devices are currently focused on the application to water distribution systems (Strathmann et al., 2013). However, other deployment applications are emerging. Such monitoring is applicable to many fields, including: cell health monitoring in bioreactors (O'Mara et al., 2018); noninvasive monitoring of cell growth in bioreactors (Reinecke et al., 2017); online biofilm monitoring of cell density (Qiu et al., 2014); and micro-biosensors for batch-fed fermentation with integrated online monitoring (Buchenauer et al., 2009). Similar deployment of this technology is used by environmental microbial sensors. These produce utilize microbial electrochemical cell technologies, producing energy from water that contains high organic content (Du et al., 2007; Logan et al., 2006; Logan & Regan, 2006a, 2006b). This technology relies on microbes that establish biofilm on electrode surfaces, typically graphite or titanium (Bond & Lovley, 2003; Logan, 2009). Electrons are transferred from microbes to an anode in biochemical mechanisms (Reguera et al., 2006; Schröder, 2007). When operating with a closed circuit, electrons flow from the anode to the cathode, with the ultimate electron acceptor commonly atmospheric oxygen near the cathode.

This electrical current serves as a metric to determine the concentration of a substrate near the anode, useful in the development of microbial sensors that measure electrical currents in an aquatic environment (Kara et al., 2009; Lei et al., 2007; Mulchandani et al., 2006). In wastewater applications, organic carbon concentration can be determined by correlating the electric current between the anode and the cathode

(Dhall et al., 2008; Kim et al., 2003). However, these closed-circuit technologies result in accumulated internal resistance, decreasing the sensitivity and reliability of the sensor (Cai & Wang, 2010; Punter et al., 2013).

In wastewater treatment facilities, the operation performance may be evaluated using MPS. The relationship between carbon loading, oxidation-reduction potential, and dissolved oxygen can be monitored to evaluate the reduction in biological oxygen demand. An increase in MPS signal indicates an increase in biological oxygen demand (Burge et al., 2020). Patterns from MPS were more repeatable and defined than those of the dissolved oxidation and oxidation-reduction potential sensors (Burge et al., 2020). The communication of increasing biological oxygen demand is useful to operators of the wastewater treatment facility, and when one of the MPS did not follow the same pattern as the others (Burge et al., 2020), this indicates the spatial capability of the technology to assess homogenous treatment.

The effect of toxic metals on biofilms has been observed with MPS. Selenium, lead, arsenic, nickel, silver, cadmium, and zinc solutions were introduced into a model bioreactor, where response data was assessed using MPS signal generation and inhibition of signal (Brown et al., 2020). These metals were selected as they are representative of toxic metal compositions entering the international wastewater treatment facility at the United States/Mexico border (Lester & van Riper III, 2014). Electron generation and cytochrome storage is inhibited by toxic metal constituents (Burge et al., 2020). When the toxic metals were eliminated from the system, the inhibitory effects were removed, allowing normal metabolic activities to resume. This can be observed by an increase in

the microbial open-circuit potential. The high correlation between metal concentrations and microbial response indicates the potential for the sensors to quantify metal concentrations. While the sensitivity of the electrodes may vary due to the surface biofilm composition, each sensor is capable of responding to conditions in the same manner (Brown et al., 2020). The ability of MPS to detect changes in toxic metal concentrations in real-time assists enforcement and operators to prevent and mitigate toxins in processing. Water resources and the systems that rely upon them are threatened by toxic metal pollution (S.-L. Wang et al., 2013), and many operations that use toxic metals do not utilize treatment to prevent the discharge of these metals (Geng et al., 2014; Pareek, 1992).

Another similar sensor technology utilizing flavin-phenol composite film has measured pH *in situ* (Casimero et al., 2018). The redox chemistry of the flavin group serves as an electrochemical mediator in a range of chemical (Radzevič et al., 2016) and microbial systems (Bao et al., 2016; Si et al., 2016; Wu et al., 2015; Yu et al., 2017). This sensor is an advancement of small, flexible, and robust *in situ* pH sensor predecessors (Salvo et al., 2017; J. Yang et al., 2016). Electrochemical responses were compared to observations made with a conventional glass electrode (Casimero et al., 2018). In a fresh pH buffer of 7, redox processes were stable. This is as expected at constant equilibrium conditions (Burge et al., 2020). The relationship between peak position and pH was found to be near Nernstian with a slope of 55 mV/pH unit. The pH of the fermentation medium fell from a pH of 6.18 to a pH of 3.68 when complete. Despite abnormalities, the flavin pH recordings followed those obtained with the conventional glass probe. Significant

deviations occurred only after the electrode was dormant for over 12 hours. It was suspected that during this dormancy, microbial colonization on the probe compromises the pH response within the biofilm interface (Casimero et al., 2018). Biofilm formation is apparent after 51 hours, which may be problematic when transferring results to other microbial systems (Y. Yang et al., 2015) and should not be used as a direct reference for this research.

In cultivating S*accharomyces cerevisiae*, a single-celled fungal microbe of yeast, Favre and colleagues utilized a graphite electrode for biosensing (Favre et al., 2009). Graphite was selected as it was an inexpensive, disposable, and sufficiently conductive material without further surface treatment; all desirable characteristics in developing biosensors (Favre et al., 2009; Stoianov et al., 2008). An abiotic cathode is used for biosensing as it ensures stable potential as microbes grow. The cathode serves as a working or reference electrode, creating a different potential from the sensing electrode. The yeast's ability to process glucose and fructose into ethanol was monitored with potentiometric and conductivity measurements recorded with a datalogger every four minutes. Glucose and fructose concentrations were measured as well. A bioreactor was constructed to contain the experiment, with two sensing electrodes integrated into the reactor's design. Using multiple potentiometric sensors to record signals, one electrode was used as the working reference electrode. Conductivity was found to remain steady and low for the duration of the experiment, with the end of the fermentation process and microbial cultivation noted by a decrease in voltage and current values (Favre et al., 2009). The amperometric signal decreased to a nadir then increased, indicating the yeast

microbes began to consume other nutrients. This indicates that the sensor is capable of recording microbial metabolism and metabolic activity, determining when metabolism is complete. The experimentation yielded good reproducibility for the bioelectrochemical measurements, demonstrating microbial fuel-cell-type activity sensors to be a valuable tool for monitoring a microbial culture. The potentiometric signals indicating real-time microbial activity and the progression of carbohydrate conversion by the microbes is directly relevant to this research.

Another study monitored the growth of biofilms with a graphite potentiometric sensor (Poma et al., 2020). Here, *E. coli* and *P. aeruginosa* have been reported as electrochemically active (Sydow et al., 2014), electrons transferred through electron mediators and phenazine derivatives, respectively. All tested strains of *E. coli*, *P. aeruginosa*, and *S. aureus* were able to form biofilm in the presence of a culture media. The open-circuit potential changed over time, shifting towards a negative potential value as the bacteria grew. A significant negative correlation with the optical density value and bacterial growth was observed (Poma et al., 2020). Furthermore, the potentiometric sensor system was able to distinguish the different phases of bacterial growth. The open-circuit potential in the negative control did not change over time, validating the association with the bacterial growth process. The presence of defects on the chemical reduction graphene oxide sensor did not impair the electrical conductivity, and may potentially provide reactive sites for biofilm adhesion and electron transfer (Poma et al., 2020). The low current flowing between the working and reference electrode allows open-circuit potential measurement to be an ideal electrochemical transduction technique

for biofilm monitoring due to the negligible effects on bacteria (Janknecht & Melo, 2003). A significant positive correlation between bacterial growth, in colony forming units (CFUs) per cubic centimeter and the optical density was found (Poma et al., 2020). The bacterial concentrations detected on the electrode surface is close to the non-healing threshold of skin wounds (Bowler, 2003). As such, the bacterial concentrations on the electrode may provide a good approximation of the bacterial colonization that would occur as a wound is infected. This allows for monitoring and early detection of microbial colonization and may therefore avoid the undesired effects of infections. The sensor may be embedded into clinical and medical applications for rapid detection of biofilms formed by bacterial species of importance.

An electrochemically reduced graphene oxide electrode was operated as a pH sensor during experimental fermentation of *L. lactis*, used in the production of dairy products (Chinnathambi & Euverink, 2019). The culture medium was prepared, inoculated, and cultured with pH measured continually until the optical density of the culture was constant, indicating no growth of the bacteria. With the electrode in the culture, current initially decreased before reaching a stable value. Once bacterial growth began, current gradually decreased. The current decrease was accelerated during the exponential growth phase of *L. lactis* until a stable end value was reached and growth stopped. This informs of a pH pattern related to bacterial growth in this fermentation process that may be observed in this research.

To sense the content of tyramine in dairy products, Draz and coworkers developed and optimized a sensor to rapidly test these products for quality and safety

(Draz et al., 2021). Tyramine is a vasoactive biogenic amine in food products that may result in life-threatening physiological reactions when consumed in high levels. Potential measurements were recorded using a potentiometric model, consisting of a double electrode system: a working electrode and a silver-silver chloride reference electrode. This system measures the difference in potentials, and is combined with a pH glass electrode. Responsiveness of the sensor was determined by consecutive changes in tyramine concentrations. The time required for the sensor to reach a stable response was determined. The effect of pH on the measured potential was monitored through a known tyramine solution. The pH of the solution was altered, with pH and mV monitored after each minute alteration. Measured potential in mV was then correlated to the pH.

The presence of absence of the exotoxin *staphylococcus aureus* was determined by measuring the potential difference between a silver-silver chloride electrode and a PVC electrode of the sensor system developed by Ahari and colleagues (Ahari et al., 2017). This system indicates the sensor's response to the presence of the bacterial exotoxin (Z. Bai et al., 2016; Domenech et al., 2013; Singh et al., 2014). The potential of each dilution was recorded by a potentiometer. The Nernst relationship applies when the potential difference between two dilutions is 59 mV, and the reading of the electrode will become higher in the next dilution (Ahari et al., 2017). If the potential difference between two dilutions is 59 mV, then the standard Nernst slope applies, indicating that the sensor registered the presence of the exotoxin in that dilution. Should the potential difference between two successive dilutions be less than 59 mV, then the sensor would be determined to not be sensitive enough to detect the presence of the exotoxin (Yoo et al.,

2016). Similarly, the effect of temperature on the sensor's response is based on the Nernst equation; temperature was measured between 2 ºC and 35 ºC (Ahari et al., 2017). Results were plotted by recording the signals (Eftekhari-Sis et al., 2016). This sensor was unable to distinguish between one dilution and more-diluted solutions (Ahari et al., 2017). Potential differences remained constant in the pH range of 5.0 – 8.5. The sharp change in potentials at higher pH may be attributed to the deprotonation of free carboxyl groups (Ahari et al., 2017). Changes in potential at lower pH values is related to the protonation of the amine groups of the exotoxin. From this, it may be inferred that the charge-transport process of the sensor due to a higher concentration of hydronium ions lowers pH. Despite an inherent detection limit for this sensor, the sensor could be employed to determine the presence of *S. aureus* without interference.

Electron transfer itself was investigated by Otero and associates with a working electrode, a graphite counter electrode, and silver-silver chloride reference electrode (Jiménez Otero et al., 2021; Yates et al., 2018). Response time of the biofilm was also calculated from the Nernst equation, where conductivity was characterized to describe the degree to which the biofilm conducts electrical current by redox electron transfer (Jiménez Otero et al., 2021).

A lack of research remains in the field of bacterial-toxin detectors using biosensors. A variety of health deployment opportunities remain for these. For example, similar sensors were able to detect the West Nile virus protein at a pH of 7 (B. T. T. Nguyen et al., 2009).

MPS have yet to be directly applied to the real time monitoring of microbial activity in anerobic fermentation, such as the culturing of yogurt. In this process, potentiometric signals may be interpreted to determine microbial bioactivity. Nonetheless, Casimero and coworkers tested pH monitoring in a complex and changing system (Casimero et al., 2018). The solid-state pH sensor was demonstrated to be capable of operating in a microbial reactor. Clear signals with redox peaks were produced, from which pH can be computed. The system is reagent-less and inexpensive, features shared with MPS (Favre et al., 2009; Stoianov et al., 2008).

Microbial Fermentation Reactions and Yogurt Production

Fermented milk products are obtained by the fermentation of milk by specific microorganisms. According to the International Food Standards published from the Food and Agriculture Organization (FAO), fermented milk is a product that is obtained by the fermentation of milk, which may be manufactured from products obtained from milk with or without compositional modification by the action of microorganisms and resulting in the reduction of pH (FAO, 2018). This change in pH will be monitored in this research. A fermentation medium is a chemical environment that includes peptides, salts, and redox molecules that interfere with a sensor's surface (Ambrosi et al., 2014; Z. Wang et al., 2016; F. Xie, Cao, et al., 2018; F. Xie, Liu, et al., 2018; L. Xie et al., 2017). Beyond microbial growth, milk is also subjected to oxidation of fatty acids and the evaporation of volatile organic compounds that may have had an unmeasured effect on an experimental system (Winquist et al., 1998). Starting microorganisms should be viable,

active, and abundant in the product. The starting milk itself must be fresh and sanitary, with low bacterial counts and absent of pathogens and antibiotics, sanitization residues, and other inhibitors (de Oliveira, 2014).

Kefir is produced by culturing milk with kefir grains, a heterogeneous mixture of lactic acid bacteria, acetic acid bacteria, and yeasts contained in an exopolysaccharide matric (Rosa et al., 2017). The probiotic nature of kefir has numerous health benefits (Bourrie et al., 2016; Fiorda et al., 2017; Gul et al., 2015; Laureys & De Vuyst, 2014, 2017; Rosa et al., 2017; Satir & Guzel-Seydim, 2016) with a long history of production and consumption.

The resulting beneficial health properties of fermented milk products have been known for years; Russian bacteriologist Elie Metchnikoff was the first to explain the beneficial effects of lactic acid bacteria that is present in fermented milks (de Oliveira, 2014). However, Metchnikoff showed that *L. bulgaricus*, a bacteria used in this research, does not survive and does not colonize the gastrointestinal tract. Other probiotics in fermented products have been documented to have a beneficial effect through the growth and action in the gastrointestinal tract (de Oliveira, 2014). In yogurt, this is achieved with the living probiotic microorganisms, nondigestible prebiotic carbohydrates, and bioactive metabolites. Probiotic microorganisms belong to the genera *Lactobacillus, Bifidobacterium, Streptococcus,* and *Saccharomyces.* Benefits of probiotic microorganisms include increased immune modulation and prevention of disease and infections, especially related to intestinal, breathing, and urinary infections (de Oliveira, 2014). As such, probiotic bacteria should be present in final yogurt products at high

viable counts for the duration of the yogurt's shelf life. At the same time, it is evident that in heat treatment of yogurt, *L. bulgaricus* and *S. thermophilus* starter cultures are destroyed. Therefore, yogurt must contain an abundant and viable population of these bacteria, or the final product cannot be called yogurt according to these standards.

Dairy product fermentation has recently been aided by scientifically-based manufacture and controlled fermentation. This process has been further aided by the improvement of knowledge in microbiology, enzymology, physics, engineering, chemistry, and biochemistry (de Oliveira, 2014). Processing conditions including pH, temperature, and fermentation time influence the nutritional characteristics of the products (Ntsame Affane et al., 2011; Satir & Guzel-Seydim, 2016). Lactic acid is produced by microbes during the fermentation process (Fiorda et al., 2017). During culturing, the mixture composed of molecules, minerals, proteins, and fats exchange with the growing kefir grain biomass (Casimero et al., 2018). The monitoring and control of pH during production thus allows for greater control over some aspects of the final product characteristics and qualities (Ntsame Affane et al., 2011; Satir & Guzel-Seydim, 2016). Yogurt itself may take on a variety of these different final characteristic structural properties. Of these, set yogurt is where fermentation takes place inside a package (de Oliveira, 2014) and is most similar to the process used in this research.

As the bacterial communities transform the milk, pH will decrease, typically from a pH of 6.5 to a pH of 3.5 (Bause et al., 2018). At the same time, viscosity will increase, which may result in surface fouling (Casimero et al., 2018). These microbial interactions in food processing affect the final product (Dantism et al., 2019). Similarly,

microorganisms in soy sauce enhance the aroma and flavor profile of the final product during the fermentation process (Devanthi & Gkatzionis, 2019). In the fermentation of coffee, mucilage is degraded into alcohols, acids, and enzymes by microorganisms, impacting the product's final quality (Haile & Kang, 2019). During the shelf life of yogurt, the number of bacteria decreases as the product's acidity increases (de Oliveira, 2014), which frequently leads to undesired off-flavors.

Yogurt products in particular have expanded as a result of food technology and research, including the development of new ingredients. Yogurt products may have better market acceptance, and thus greater profit and safety, if manufacturers invest more into understanding characteristics of the product, including texture, taste, and health-related probiotics (de Oliveira, 2014). Yogurt is classified as a product that includes the fermentation of probiotic cultures of yogurt, including fermentation products that take place with photosymbiotic cultures of *S. thermophilus* and *L. delbrueckii* subsp. *Bulgaricus* (de Oliveira, 2014). These cultures may be accompanied by other lactic acid bacteria that may contribute to the activity and determine final product characteristics.

Streptococcus thermophilus and *L. bulgaricus* are yogurt bacteria adapted for growth in milk. Milk provides a good matrix for these microorganisms, containing approximately 47 g/mL carbohydrates, 36 g/mL fats, and 33 g/mL proteins (de Oliveira, 2014), as well as a variety of vitamins and minerals. Each of these components are critical for the production of fermented milk. Calcium and phosphorous, for example, are essential minerals for the formation of the characteristic gel structure of yogurt (de Oliveira, 2014). These microorganisms have enzymes and metabolic pathways that use

lactose as an energy source for the starter culture, as well as proteinases and peptidases that enable the assimilation of nitrogen for cell growth (de Oliveira, 2014). The addition of other ingredients affects the final yogurt product as well. For example, the incorporation of sugar increases the time it takes to reach the final pH, due to an inhibitory effect of bacteria with an adverse osmotic effect as well as low water activity (de Oliveira, 2014). For this reason, sugar or any other additional ingredients will not be added to the yogurt that is produced in this research.

A series of heating and cooling standardizes milk before culturing to provide an appropriate environment for fermentation. This homogenizes milk and milk solids to promote the uniform dispersion of fat in the milk mixture. In turn, this increases the viscosity and improves the characteristic qualities of yogurt (de Oliveira, 2014). Heat treatment is thus one of the main parameters that effects the texture, structure, and rheology of the final yogurt product. Milk is heated to a temperature between 85 ºC and 95 ºC, depending on the desired final texture. Following heat treatment, the milk is cooled to a temperature appropriate for the inoculating bacteria to proliferate, typically lower than 42 ºC (de Oliveira, 2014). Then, an inoculum concentration between 1% and 5% is added depending on the starter's manufacturer, however minimum inoculations are recommended to prevent an intense acidification (de Oliveira, 2014). This research will follow a lower inoculum concentration to avoid this acidification.

Fermentation time varies between 4 and 20 hours until a final pH of around 4.3, the isoelectric point where the milk's casein becomes unstable and coagulates, forming yogurt's distinctive firm gel (de Oliveira, 2014). Whey protein is trapped within this gel

matrix, with higher whey protein milk yielding stronger gel yogurt. Fermentation is stopped by finally cooling the yogurt to 5 ºC. This cooling reduces metabolic activity of the culture and controls further acidification of the product.

In a previous study, a solid-state pH sensing element with a microbial reactor was designed for use in kefir fermented milk products (Casimero et al., 2018). Before this, an electronic tongue was used to monitor the freshness of milk (Winquist et al., 1998). This electronic sensor monitored the deterioration of milk quality due to microbial growth at room temperature. Milk serves as an ideal growth medium for several groups of bacteria, of which the selected microbes for this research will be selected. Winquist and colleagues placed working and reference electrodes of the electronic sensor into the milk reactor. This sensor array, however, required an electrochemical procedure to clean the working electrode, which is not required when using MPS. Samples were measured around room temperature, between 21 ºC and 25.5 ºC (Winquist et al., 1998), which will be used to inform this research. At different temperatures, different microbial constituents may be promoted, and as such, measurements of the total bacteria content may be made without identifying the individual composition of bacteria (Winquist et al., 1998). Further, no precautions were made to prevent microbial growth in the milk samples. Interestingly, despite using different packages of milk, samples at the same temperature were observed to have similar microbial measurements, and likely contained different starting bacterial contents (Winquist et al., 1998). Winquist and colleagues conclude that the simplicity and durability of the voltametric sensing system provides a potential that may be further paired with other electrochemical parameters, namely conductivity, furthering the

possible applications of such sensors and ushering the expectations of MPS and other developed sensor technologies.

Similar to this research, Chinnathambi and associates developed an electrochemically reduced graphene oxide electrode that operated as a pH sensor during the fermentation of *L. lactis* (Chinnathambi & Euverink, 2019). This bacteria produces lactic acid and is used to ferment food. During fermentation, the production of this lactic acid lowers the pH of the process, until the bacterium stops growing at a low pH (Britton & Robinson, 1931; Hols et al., 1999; Luedeking & Piret, 1959). During *L. lactis* growth, glucose is converted into biomass and lactic acid that decreases the pH of the fermentation process. Growth ends when the pH of fermentation is too low to support proper growth or when no glucose remains to be converted (Chinnathambi & Euverink, 2019).

CHAPTER 3

METHODOLOGY

Experimental Design and Methods

Organic whole milk (WinCo Foods, USA) was fermented in an open-top 500 mL glass reactor vessel. This type of milk was selected as it would be free of excess antibiotics, which may interfere with or impede proper microbial culturing (de Oliveira, 2014). Two 50 mm long cylindrical carbon (fiberglass reinforced) MPS electrodes with a diameter of 5 mm (Burge et al., 2019) were placed in the vessel parallel to each other at the bottom of the reactor. A traditional oxidation-reduction potential (ORP) probe was placed between the two electrodes was connected to the MPS data collection system to obtain simultaneous reference data. The spatial positioning of these probes and MPS electrodes prevents contact with each other while also capturing the entire vessel's contents, as seen in Figure 1. Further, using two electrodes allows the average of the recorded signal to be calculated for a more representative capture of the process. The ORP probe also functioned with a secondary silver-silver chloride reference electrode, which would serve as the reference electrode for both the MPS and ORP electrodes.

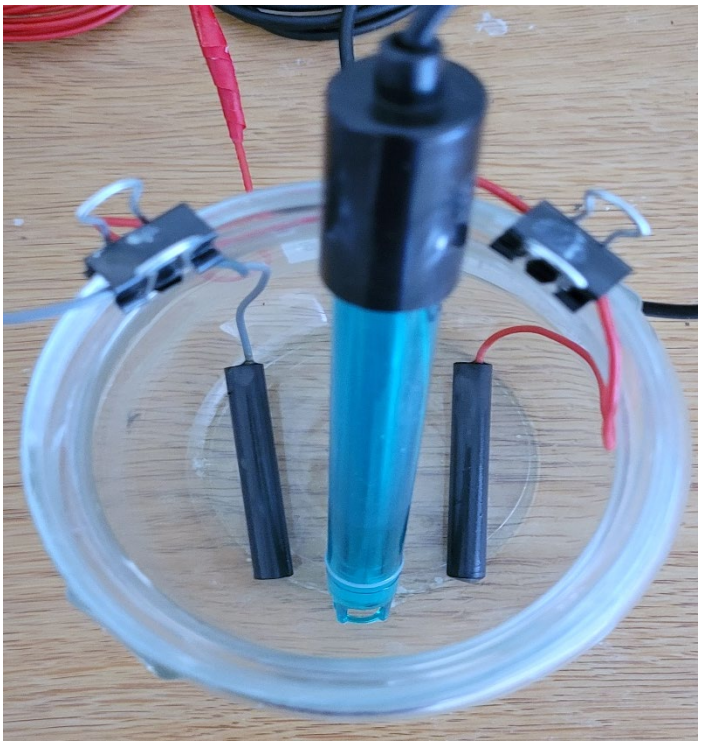

Figure 1. Electrode Setup. The open-top vessel containing the grey (left) and red (right) carbon tube MPS electrodes and the silver-silver chloride reference electrode in the ORP probe (center).

The OCP data collection system was developed by Dr. Dragan Boscovic and his team (Vizcore LLC, Scottsdale, AZ, USA). The system automatically collected data at a frequency of every 69 seconds. This frequency ensures the system captures a snapshot of the process every minute to provide a true and real-time profile of the reaction. An independent pH probe (Beckman Coulter, Brea, CA, USA) was used to obtain pH reference data at regular intervals, typically capturing an average of 23 pH readings during each fermentation experiment. pH is also obtained to use in tandem with MPS signals to distinguish fermentation completion, where the decrease of pH from the

production of lactic acid, continuing fermentation until the bacteria stops growing at a low pH (Britton & Robinson, 1931). Photographs were taken to observe visible changes in the milk's structure and the development of biofilm on the sensors at various stages of the fermentation process. Before each experiment, all electrodes and probes were washed with reverse-osmosis treated water, as well as gently brushed to remove any accumulated biofilm, yogurt gel, or milk solids. This would ensure standardized measurements for each experimental run. The pH probe was calibrated using a standard 3-point buffer calibration method. Further, the pH probe was rinsed with reverse-osmosis treated water between readings. A log containing the inoculation amount, time, pH, and temperature was maintained for each experiment to be paired with the MPS and ORP collected data.

A set of four experiments were conducted. In each experiment, 200 mL of milk was first subjected to a heat treatment. Heat treatment was conducted in a hot water bath to reach a temperature of at least 75 ºC (de Oliveira, 2014). This step results in a modification of the physical-chemical properties of denatured casein and whey proteins, releasing products that stimulate the growth of the cultures, removing dissolved oxygen in the milk, improving the growth of microaerophilic cultures, and killing potential pathogenic microorganisms that may be present in the milk (de Oliveira, 2014). Next, the milk was cooled to 42 ºC for the inoculation of the cultures (de Oliveira, 2014). A 10mL aliquot of milk was measured to weigh 10.3 grams, as such the density of the milk used was found to be approximately 1.03 g/mL. This density was used to determine the inoculation dose for a 1% inoculation mass/volume ratio. For 200mL of milk, 2.04 g of a lyophilized culture blend containing *L. acidophilus*, *L. bulgaricus*, and *S. thermophilus*

was completely mixed into the milk, achieving the 1% inoculum-to-milk concentration (de Oliveira, 2014). This is the recommended minimum inoculation ratio, selected to prevent intense acidification of the mixture (de Oliveira, 2014). The mixture was kept at 23 ± 2 ºC during the fermentation process and monitored using a traditional glass thermometer. pH was recorded regularly until the a of pH = 4.3 approached and stabilized. The isoelectric point of the inoculated milk is where acidity of the fermentation mixture reaches 1.0 g of lactic acid per 100 mL of the mixture (de Oliveira, 2014), destabilizing the milk's casein and coagulating the mixture to form yogurt's characteristic gel structure. Depending on the milk's protein content, the isoelectric point may vary from a pH of 4.7 to as low as a pH of 4.0 (de Oliveira, 2014); however, using pH = 4.3 is an approximate midpoint and would ensure the pH of the mixture would proceed beyond the upper reach of this typical isoelectric point range. At the end of each experiment, all electrodes and probes were removed and washed with reverse-osmosis treated water, as well as gently brushed to remove any accumulated biofilm, yogurt gel, or milk solids. The glass reactor vessel was also completely washed between experiments and rinsed with reverse-osmosis treated water.

Preparation and Assembly of Data for Primary Analysis

Data collected by the automatic data collection system was assembled into a database for analysis and interpretation. The timestamped data was extracted for each experimental run, starting with the initial time of inoculation and ending with the last recorded pH reading. The open-circuit potential measured by the red carbon tube (1) and

grey carbon tube (2), in volts (V) was determined by subtracting the output of the resulting average (3) of the two carbon MPS electrodes from the time-corresponding output of the secondary silver-silver chloride reference electrode of the ORP probe.

$$\Delta E_{OCP,\ Red} = \Delta E_{CarbonTubeRed} - \Delta E_{REF,\ Ag/AgCl} \quad (1)$$

$$\Delta E_{OCP,\ Grey} = \Delta E_{CarbonTubeGrey} - \Delta E_{REF,\ Ag/AgCl} \quad (2)$$

where

ΔE_{OCP} = Open-circuit potential measured by the carbon tube electrode in volts

$\Delta E_{CarbonTube}$ = Data value recorded by the carbon tube electrode

$\Delta E_{REF,\ Ag/AgCl}$ = Theoretically constant value recorded by the silver-silver chloride reference electrode, approximately 1.67 volts

$$\Delta E_{MPS,\ Average} = \frac{\Delta E_{OCP,\ Red} + \Delta E_{OCP,\ Grey}}{2} \times \frac{1000\ mV}{1\ V} \quad (3)$$

where

$\Delta E_{MPS,\ Average}\ (mV)$ = The average MPS signal of the red and grey carbon tube electrodes in millivolts

$\Delta E_{OCP,\ Red}$ = Open-circuit potential measured by the red carbon tube electrode in volts

$\Delta E_{OCP,\ Grey}$ = Open-circuit potential measured by the grey carbon tube electrode in volts

This calculation was performed for each recorded time before voltage was converted to millivolts (mV). Each data point's logged time was converted into seconds (s) and minutes (min), with the initial inoculation time becoming t = 0 sec. The pH values were entered into the database at the corresponding timestamps. Temperature was assembled at the appropriate timestamps alongside the pH capture points.

This assembly of MPS mV output, pH, temperature, and time was thus prepared for graphical analysis. A scatter chart was plotted, with time in minutes on the x-axis and the MPS signal (ΔE, in mV) on the y-axis. Recorded pH measurements were added at their respective timestamps. This presented a graph that displays the change in MPS signal output over time with the related pH measurements. Each experiment was graphed in this manner, with all experiments then colligated into a single graph to determine the average MPS signal over time.

Guided by this assembly, fermentation completion times were determined. Slope was calculated (4) in consecutive groupings of 15, 10, and 5 timestamped data points to provide different resolutions, corresponding to approximately groupings of 15, 10, and 5 minutes, respectively. Equation (4) will result in a value of zero when there is no change in the averaged MPS signal throughout the consecutive grouping's timeframe.

$$b = \frac{(t-\bar{x}_t) \times (\Delta E_{MPS,\ Average} - \bar{x}_{MPS})}{\sum(t-\bar{x}_t)^2} \quad (4)$$

where

b = slope

t = the single timestamp of each data measurement

$\bar{x}_t$ = the average of the 15, 10, or 5 minute grouping

$\Delta E_{MPS,\ Average}$ = the average MPS signal as calculated in (3) of each data measurement in millivolts

$\bar{x}_{MPS}$ = the average MPS signal of the 15, 10, or 5 minute grouping

When the slope result approaches zero and often results in the minimum value of the slope calculation, fermentation was determined to be complete at a moment where the signal does not change. This equation will result in a zero value for each instance there is no change between consecutive MPS signal recordings; as such, there may be multiple regions of zero values. Consideration as complete fermentation would thus be limited to the data with a pH below 5.0 and a slope resulting in relative zero values.

In the absence of pH data between two recorded pH points, the previous and following pH measurements were linearized to calculate an estimated pH within this range (5). This was performed as needed in areas with no recorded pH to assist in determining the pH during a timeframe where fermentation was potentially complete.

$$\mathrm{pH}_{t_x} = \left(\frac{\mathrm{pH}_{t_2} - \mathrm{pH}_{t_1}}{t_2 - t_1}\right) \times (t_x - t_1) + \mathrm{pH}_{t_1} \quad (5)$$

where

pH_{t_x} = the estimated pH at the desired time x

t_x = time x in minutes

t_1 = time of pH_1 in minutes

t_2 = time of pH_2 in minutes

pH_{t_1} = pH at time 1

pH_{t_2} = pH at time 2

Using calculated or measured pH and the plotted time vs. MPS signal graph would further limit the range where fermentation was expected to be complete, visually with a plateau in MPS signal. This range would then be examined with the calculated slopes and average MPS output to precisely determine a time of complete fermentation.

With no change in open-circuit potential as reported by the averaged MPS signal, there is no electron exchange sufficient to induce a change in the ΔE (OCP) value (Hristovski et al., 2022). In this instance of stable OCP, fermentation is complete and the isoelectric point has been reached. This temporal region is where the redox processes associated with the transfer and movement of electrons of the redox fermentation metabolic processes have slowed to nearly nothing (Hristovski et al., 2022). With the slope calculated for each consecutive recorded measurement, identification of these points of no change informs completed fermentation. However, beyond a range of this isoelectric behavior, MPS and thus calculated slope will no longer be zero as the yogurt mixture is subjected to decomposing microorganisms that will proliferate in absence of protective measures including sealing and cooling (de Oliveira, 2014).

Primary Analysis

Following the identification of the approximately zero slopes of change in MPS signal over time, complete fermentation times were determined. These time points were then assembled in a separate log, containing each experiment's inoculum mass,

timestamp of complete fermentation as described above, the corresponding approximately zero slope for that time point, the MPS signal for that time, and the pH of this complete fermentation time. pH was calculated as above using a linear function where pH was not captured at the time determined to be complete fermentation. This assembly allowed for convenient comparison across experimental trials, as well as serving as the guiding information for the primary analysis.

With the determined information organized in this method, simple initial comparison between experiments is possible. This data indicates a time snapshot of the MPS signal and pH of the reaction at the moment at which fermentation was deemed to be complete for each experiment and at with each inoculum masses. From here, the average values for time (6), MPS signal (7), and pH (8) at each experiment's time of complete fermentation were calculated from the four experiments.

$$\bar{x}_t = \frac{\sum(t_1 + t_2 + \cdots t_n)}{n_t} \tag{6}$$

where

$\bar{x}_t$= average time of complete fermentation

t_1 = time of complete fermentation in one experiment

n_t = number of experiment times to be averaged

$$\bar{x}_{\Delta E} = \frac{\sum(\Delta E_1 + \Delta E_2 + \cdots \Delta E_n)}{n_{\Delta E}} \tag{7}$$

where

$\bar{x}_{\Delta E}$ = average MPS signal at the time of complete fermentation

ΔE_1 = MPS signal at the time of complete fermentation in one experiment

$n_{\Delta E}$ = number of experiment MPS signals to be averaged

$$\bar{x}_{\mathrm{pH}} = \frac{\sum(\mathrm{pH}_1 + \mathrm{pH}_2 + \cdots \mathrm{pH}_n)}{\mathrm{n_{pH}}} \tag{8}$$

where

$\bar{x}_{\mathrm{pH}}$ = average pH at the time of complete fermentation

pH_1 = pH value at the time of complete fermentation in one experiment

$\mathrm{n_{pH}}$ = number of experiment pH values to be averaged

Standard deviation was calculated in the same manner for time (9), MPS signal (10), and pH (11). The average provides an overall range for time, MPS signal, and pH when fermentation is complete.

$$\sigma_t = \sqrt{\frac{\sum(t_i - \bar{x}_{\mathrm{t}})^2}{n_t}} \tag{9}$$

where

σ_t = standard deviation of complete fermentation time, in minutes

t_i = time of complete fermentation for each experiment

$\bar{x}_{\mathrm{t}}$ = average time of complete fermentation as calculated in (6)

n_t = number of experiment times

$$\sigma_{MPS} = \sqrt{\frac{\sum(MPS\ Signal_i - \bar{x}_{\Delta E})^2}{n_{MPS\ Signal}}} \quad (10)$$

where

σ_{MPS} = standard deviation of MPS Signal at complete fermentation time, in mV

$MPS\ Signal_i$ = MPS signal at the time of complete fermentation for each experiment

$\bar{x}_{\Delta E}$ = average MPS signal at the time of complete fermentation as calculated in (7)

$n_{MPS\ Signal}$ = number of experiment MPS signals

$$\sigma_{pH} = \sqrt{\frac{\sum(pH_i - \bar{x}_{pH})^2}{n_{pH}}} \quad (11)$$

where

σ_{pH} = standard deviation of pH at complete fermentation time

pH_i = pH at the time of complete fermentation for each experiment

$\bar{x}_{pH}$ = average pH at the time of complete fermentation as calculated in (8)

n_{pH} = number of experiment pH values

Using the standard deviation, simple 95% confidence intervals were calculated, in which based on the four sets of experimental data as assembled in this primary analysis, may be interpreted to contain the true values at complete fermentation with 95% confidence. With less than 30 experiments, the confidence intervals were constructed by first obtaining the product of the t-value of 3.182 (for 95% confidence, $\alpha = 0.025$) and the

quotient of the standard deviation divided by the square root of the number of observations. These confidence intervals were done under the assumption of normal distribution. With four experiments used in the confidence interval calculation, there were n = 4 observations, and three degrees of freedom, df = 3. Next, the average value would then add or subtract this product to obtain the upper and lower range of confidence, respectively. An identical confidence interval was be calculated for time (12), MPS signal (13), and pH (14) using the respective average values and standard deviations for these items.

$$CI_t = \bar{x}_{\mathrm{t}} \pm 3.182 \left(\frac{\sigma_t}{\sqrt{n_{time}}}\right) \tag{12}$$

where

CI_t = lower and upper bounds of the confidence interval for time, assuming normal distribution

$\bar{x}_{\mathrm{t}}$ = average time of complete fermentation as calculated in (6)

σ_t = standard deviation of complete fermentation times as calculated in (9)

n_{time} = number of experiment times

$$CI_{\Delta E} = \bar{x}_{\Delta \mathrm{E}} \pm 3.182 \left(\frac{\sigma_{\Delta E}}{\sqrt{n_{\Delta E}}}\right) \tag{13}$$

where

$CI_{\Delta E}$ = lower and upper bounds of the confidence interval for MPS signal at the complete fermentation time, assuming normal distribution

$\bar{x}_{\Delta E}$ = average MPS signal at the time of complete fermentation as calculated in (7)

$\sigma_{\Delta E}$ = standard deviation of MPS signals in millivolts at the time of complete fermentation, as calculated in (10)

$n_{\Delta E}$= number of experiment MPS signals

$$CI_{\mathrm{pH}} = \bar{x}_{\mathrm{pH}} \pm 3.182 \left(\frac{\sigma_{\mathrm{pH}}}{\sqrt{n_{\mathrm{pH}}}}\right) \quad (14)$$

where

CI_{pH} = lower and upper bounds of the confidence interval for pH at the complete fermentation time

$\bar{x}_{\mathrm{pH}}$ = average pH value at the time of complete fermentation as calculated in (8)

σ_{pH} = standard deviation of pH values at the time of complete fermentation, as calculated in (11)

n_{pH}= number of experiment pH values

Method Detection Limit Calculation

The MDL was calculated using a similar data assembly as used in the primary analysis. For each of the four experiments, the inoculum mass and time of complete fermentation were organized. Next, the standard deviation of complete fermentation time across the experiments was calculated. In this case, the MDL uses the Students' two-sided distribution t-value for 95% confidence, four observations, and three degrees of freedom was 3.182 (α = 0.025). At last, the MDL is calculated (16) by multiplying this t-value by the standard deviation (U.S. EPA, Office of Water, 2016), here producing the

minimum amount of time that can be calculated and reported so as to have 95% confidence that the experiment's complete fermentation time is measured.

$$MDL = t_{(n-1,\ 0.95)} \times \sigma_t \quad (16)$$

where

MDL = the calculated Method Detection Limit for time, in minutes

$t_{(n-1,\ 0.95)}$ = Students' t-value appropriate for n observations and 95% confidence

σ_t = standard deviation of complete fermentation time, in minutes, as calculated in (9)

Sensitivity Analysis

A series of sensitivity analyses were conducted to assess the degree of confidence in the results of this research. A sensitivity analysis would examine how the results change when different analytical considerations are used of as changing the assembly of data (Thabane et al., 2013). The sensitivity analysis is incorporated into the fourth research objective and allows for additional interpretations of the data collected that may have different degrees of confidence.

For the first component of the sensitivity analysis, extreme outliers in any of the experiments were identified. Here, outlier experimental trials were identified as

containing numerically distant variables of inoculum mass from the remaining experimental trials. By identifying these outliers, the data was analyzed again excluding these observations that were included in the primary analysis. An outlier trial may deflate or inflate averages or other calculated values of a data series (Thabane et al., 2013), thus skewing the remaining data series and altering the resulting interpretation. Comparing the results of including any outlier trials in the primary analysis with the results of excluding these trials in the sensitivity analysis would indicate the effect of these outliers on the analysis of data.

Also related to the examination of the experimental trials for outliers, minor protocol deviations were identified. Between experiments, deviations from the standard protocol may have the potential impact of altering the experimental treatment and reducing the ability to compare data sets (Thabane et al., 2013).

Another aspect used for the sensitivity analysis was the impact of defining the point of complete fermentation differently. For the primary analysis, the exact recorded timestamp that captured an approximately zero slope of MPS signal over time in minutes, as described in the data assembly section of this chapter. In addition to defining this time as the exact moment of complete fermentation, the sensitivity analysis would examine an approximately 10-minute range that includes the timestamp previously determined to be the time of complete fermentation. By redefining this threshold of the experiment's outcome, time of complete fermentation, the sensitivity of the method was examined (Thabane et al., 2013). The sensitivity analysis was then interpreted as how much the time may vary within a range where the exact determination of complete fermentation is

contained yet still predict complete fermentation time with 95% confidence. To compare, the MPS signal change slopes of 10-minute time ranges where fermentation was completed as previously identified were calculated. In these time ranges, the original time of complete fermentation became the mean time of complete fermentation. These times were then when analyzed as a range rather than a single timepoint as in the primary analysis.

Additionally, the sensitivity analysis would also consider clustering. Clusters were identified as naturally occurring groups based on the inoculum mass used. Within these determined clusters, the data was expected to resemble a degree of relative homogeneity (Thabane et al., 2013) and experiments were collectively grouped as this cluster. By grouping experiments to compare between clusters, interpretation of results using this approach differ than those reached by examining each experiment individually. Sensitivity analysis by cluster was extended to congruent analysis of the previously described sensitivity analyses of outliers and the redefinition of complete fermentation as an exact time versus a timespan.

The last consideration in performing sensitivity analyses would be the impact of distributional assumptions (Thabane et al., 2013). By using the same inoculum mass in each trial, it was assumed that the resulting complete fermentation time should be approximately the same. Following the assembly of data for the primary analysis, it may quickly be determined if this assumption is valid. As the data for time and MPS signal is continuous, a sensitivity analysis would be conducted for time, MPS signal, and pH when compared as exact timestamp data. When examining slope data of the sensitivity analysis

as a 10-minute time range, considering the exact time of complete fermentation to be the mean, the time range was also standardized. Standardization using Z-scores is displayed in (17). The same equations were used to calculate the values of complete fermentation time, ΔE, and pH (18). This allows for comparison across experimental trials to obtain confidence intervals of the cluster (19), with each time range then calculated back to exact times following analysis (20). Clustering also examined the effect of standardizing time ranges. With each time range containing 10 data entries, combining time ranges from each experiment would allow for multiples of 10 observation sets to be analyzed. A larger data set size may be more insightful, and in turn lead to more robust results than those found in the primary analysis.

$$Z = \frac{X_{t/\mathrm{pH}/\Delta E} - \mu_{cluster}}{\sigma_{cluster}} \tag{17}$$

where

Z = the calculated Z-score of the value

$X_{t/\mathrm{pH}/\Delta E}$ = original value of time, pH, or ΔE

$\mu_{cluster}$ = average value of time, pH, or ΔE of the cluster

$\sigma_{cluster}$ = standard deviation for time, pH, or ΔE of the cluster

$$\mu_Z = \frac{\sum(Z_1 + Z_2 + \cdots Z_n)}{n_Z} \tag{18}$$

where

μ_Z = the calculated average Z-score of the cluster

Z = Z-scores of the cluster

n_Z = number of Z-scores in the cluster

$$CI_{\mathrm{Z}} = \mu_Z \pm t_{(n-1,\ 0.95)} \left(\frac{\sigma_Z}{\sqrt{n_{\mathrm{Z}}}}\right) \tag{19}$$

where

CI_{Z} = lower and upper bounds of the confidence interval for the Z-scores of time, pH, or ΔE

μ_Z = average Z-score of time, pH, or ΔE as calculated in (18)

$t_{(n-1,\ 0.95)}$ = Students' t-value appropriate for n observations and 95% confidence

σ_{Z} = standard deviation of Z-scores

n_{Z}= number of Z-scores

$$CI_{\mathrm{cluster}} = \mu_{cluster} \pm (CI_{\mathrm{Z}} \times \sigma_{cluster}) \tag{20}$$

where

CI_{cluster} = lower and upper bounds of the confidence interval for the clustered time, pH, or ΔE values

$\mu_{cluster}$ = average value for time, pH, or ΔE in the cluster

CI_{Z} = confidence interval for time, pH, or ΔE as calculated in (19)

$\sigma_{\mathrm{cluster}}$ = standard deviation of time, pH, or ΔE in the cluster

CHAPTER 4

RESULTS AND DISCUSSION

Description of Open Circuit Potential and pH Trends

Figure 2 depicts the obtained average ΔE and pH patterns from the first experimental trial using 0.508 grams of inoculum. This experimental trial tested the design and proper operation of the system. ΔE (in mV) increases slightly before dropping significantly after approximately 480 minutes, reaching a minimum of -266 mV at 700 minutes. From here, MPS signal increased slightly before stabilizing around -336 mV at 1070 minutes. Beyond this area, MPS signals varied, trending slightly higher. pH similarly increased from 6.44 at the start of the trial to 6.50, before gradually decreasing. The general pattern illustrates what is expected in subsequent trials and satisfies the second research objective by clearly providing MPS signal outputs and performance as hypothesized.

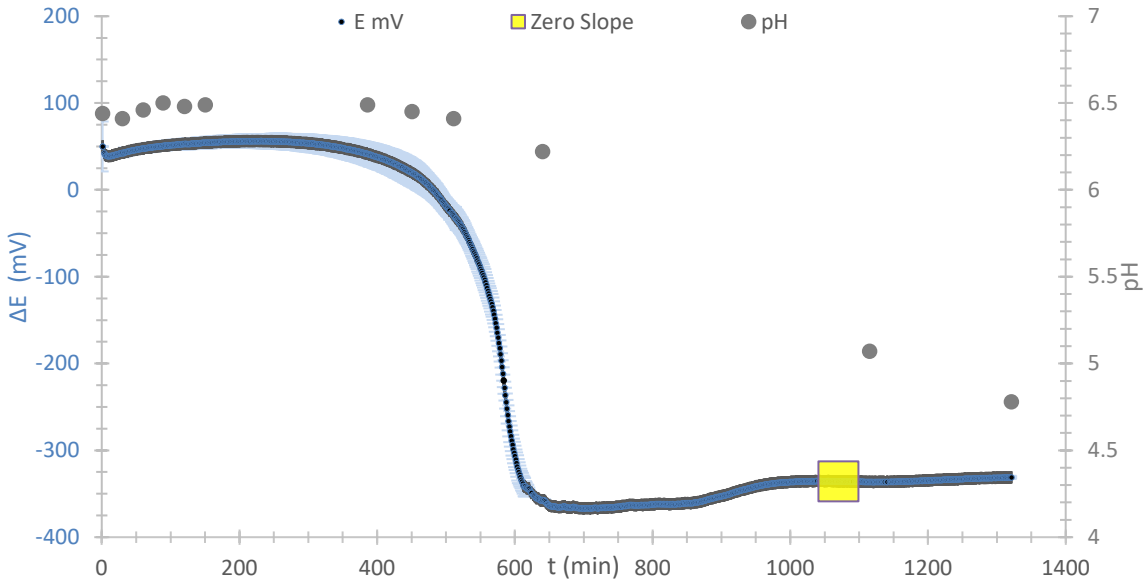

Figure 2. Initial Experimental Test with 0.508 g Inoculum Mass- Averaged MPS signal (ΔE, mV) and pH. Error bars represent the original two MPS sensor values as minimum and maximum before the average was calculated. The area where the change in energy over 10 minutes was approximately constant (zero slope) is boxed.

Figure 3 illustrates the data from the second experimental trial using 2.027 grams of inoculum. MPS signal (ΔE, mV) quickly increases slightly before dropping significantly after approximately 103 minutes before reaching a minimum of -372 mV at 432 minutes. MPS signals then steadily increased before stabilizing around -323 mV at 1468 minutes, the highest MPS signal stability value of all experiments. From here, MPS signals gradually increased. pH followed a similar pattern, increasing from 6.45 to 6.48 before steadily decreasing to 4.55. At the isoelectric point, the pH is estimated to be 4.64 using equation (5). Again this experiment supports the second research objective by confirming MPS performance and obtaining data in the yogurt medium.

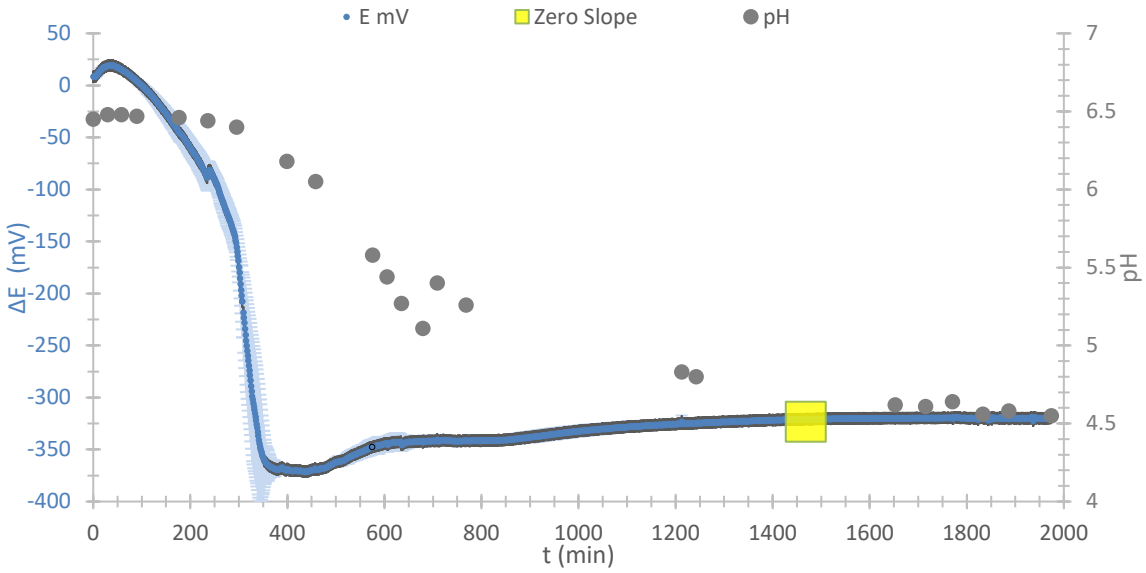

Figure 3. Average MPS Signal (ΔE, mV) and pH using 2.027 g Inoculum Mass. Error bars represent the original two MPS sensor values as minimum and maximum before the average was calculated. The area where the change in energy over 10 minutes was approximately constant (zero slope) is boxed.

Figure 4 displays the data from the third experimental trial using 2.041 g of inoculum. MPS signal (ΔE, mV) increases slightly before rapidly decreasing after 123 minutes, coming to a minimum of -362 mV at 573 minutes. MPS signal increased gradually, stabilizing around -328 mV at 1402 minutes. MPS signal remained relatively stable for the remainder of this trial. pH was closely monitored in this trial, especially nearing the stable MPS signal area. pH is estimated to be approximately 4.37 at the isoelectric point using equation (5), and was measured 4.36 less than 10 minutes later.

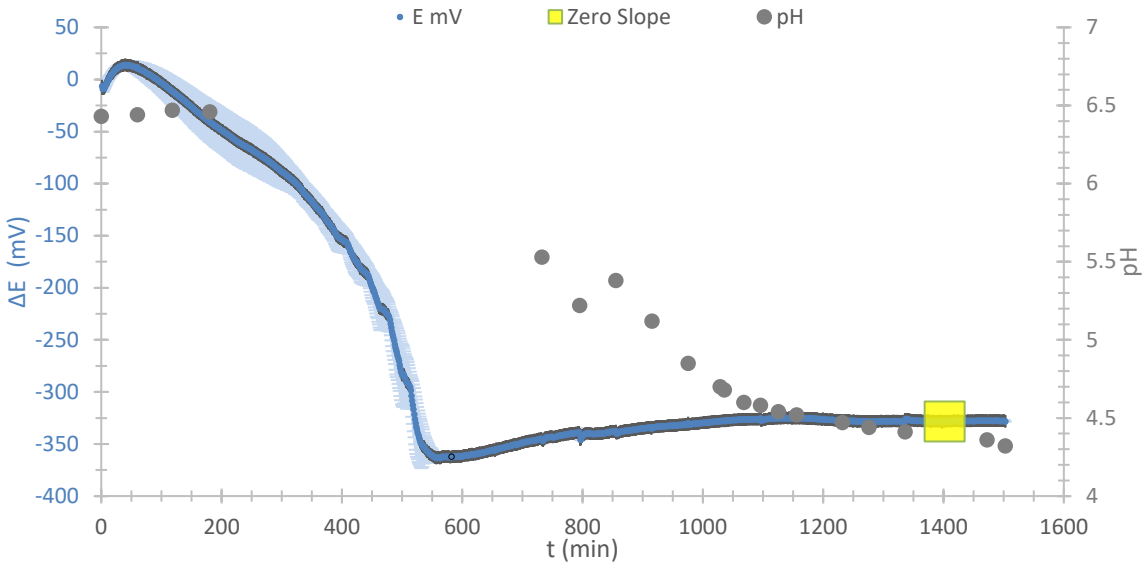

Figure 4. Average MPS Signal (ΔE, mV) and pH using 2.041 g Inoculum Mass. Error bars represent the original two MPS sensor values as minimum and maximum before the average was calculated. The area where the change in energy over 10 minutes was approximately constant (zero slope) is boxed.

Figure 5 illustrates the calculated average MPS signal (ΔE, mV) and pH patterns from the fourth experimental trial using 2.042 g of inoculum. Again, MPS signal followed a typical pattern, first increasing slightly to a maximum of 13 mV at 48 minutes, before rapidly decreasing to a minimum of -367 mV at 547 minutes. However, experiment 4 has a unique MPS signal pattern around 428 minutes, increasing slightly during the otherwise rapidly decreasing MPS signal trend. MPS signal stabilized at -333 mV around 1330 minutes before varying. The pH was observed to again slightly increase before gradually decreasing from 6.37 to 4.39, with a pH of 4.57 recorded at the end of the stable MPS signal area.

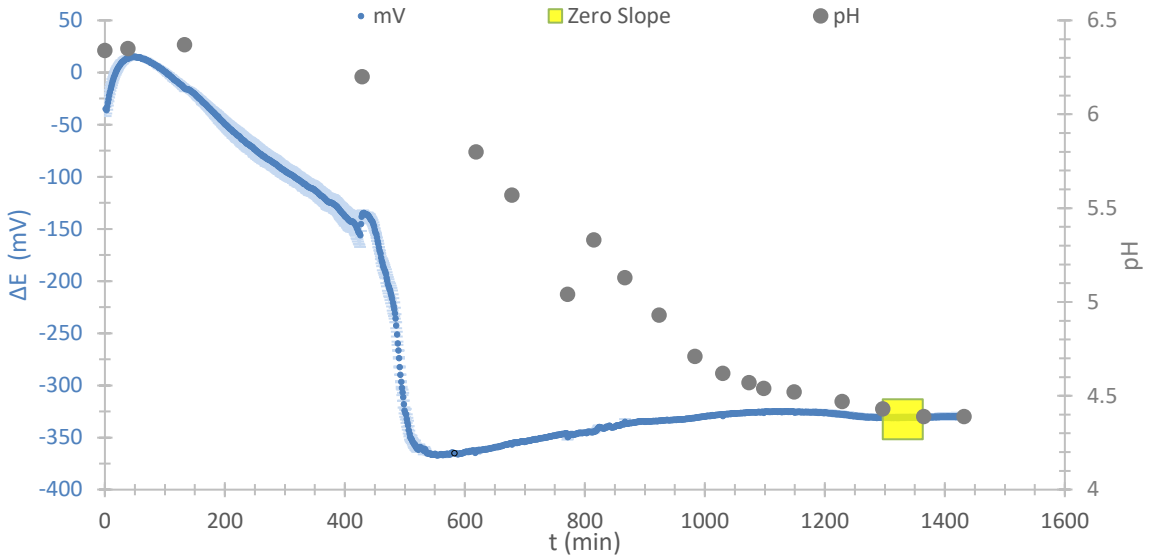

Figure 5. Average MPS Signal (ΔE, mV) and pH using 2.042 g Inoculum Mass. Error bars represent the original two MPS sensor values as minimum and maximum before the average was calculated. The area where the change in energy over 10 minutes was approximately constant (zero slope) is boxed.

Figure 6 depicts the calculated average MPS signal (ΔE, mV) and pH patterns from the eleventh experimental trial using 2.041 g of inoculum. In this experiment, MPS signals did not increase at the start as have been observed in previous trials, rather only increasing by at most 7 mV before decreasing dramatically to a minimum of -375 mV at 800 minutes. MPS signal then gradually increased before stabilizing around -333 mV, very similar to experiment four, at 1642 minutes. Beyond this area, MPS signals became sporadic, increasing slightly but rapidly before decreasing and repeating this pattern again. This may be the MPS signal capturing microbial degradation activity beyond the completion of fermentation. pH remained stable at the beginning of the experiment,

reaching a relative maximum of 6.59 before steadily decreasing to a minimum of 4.46. pH was again closely monitored at the beginning and end of this experimental trial. The pH is estimated to be 4.81 as calculated by equation (5) at the stable MPS signal range, yet continually decreased beyond this area.

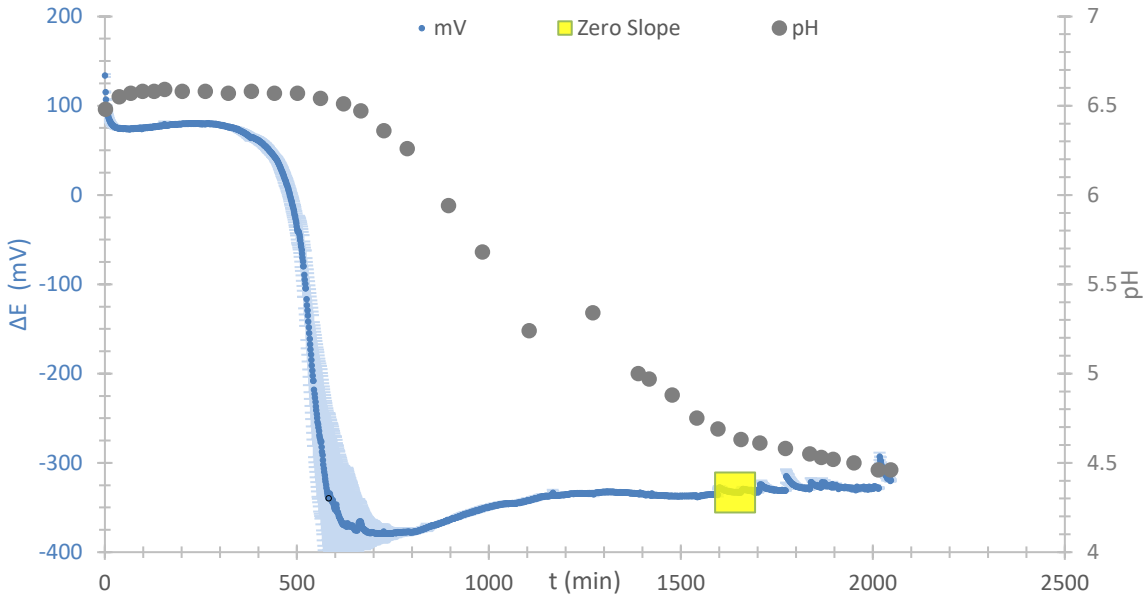

Figure 6. Average MPS Signal (ΔE, mV) and pH using 2.041 g Inoculum Mass. Error bars represent the original two MPS sensor values as minimum and maximum before the average was calculated. The area where the change in energy over 10 minutes was approximately constant (zero slope) is boxed.

Figure 7 displays the data from the twelfth experimental trial using 2.043 g of inoculum. Calculated average MPS signals (ΔE, mV) briefly increased before decreasing after 24 minutes. ΔE then gradually declined to -365 mV at 607 minutes, similar to the -367 mV of experiment 4. From here, MPS signal slowly increased before stabilizing

around -331 mV at 1244 minutes. Beyond this stable region, MPS signal slightly decreased slowly. pH was closely recorded during the rapid decrease in pH for this experiment, decreasing from 6.58 to 4.39, and measured to be 4.45 in the stable MPS signal range.

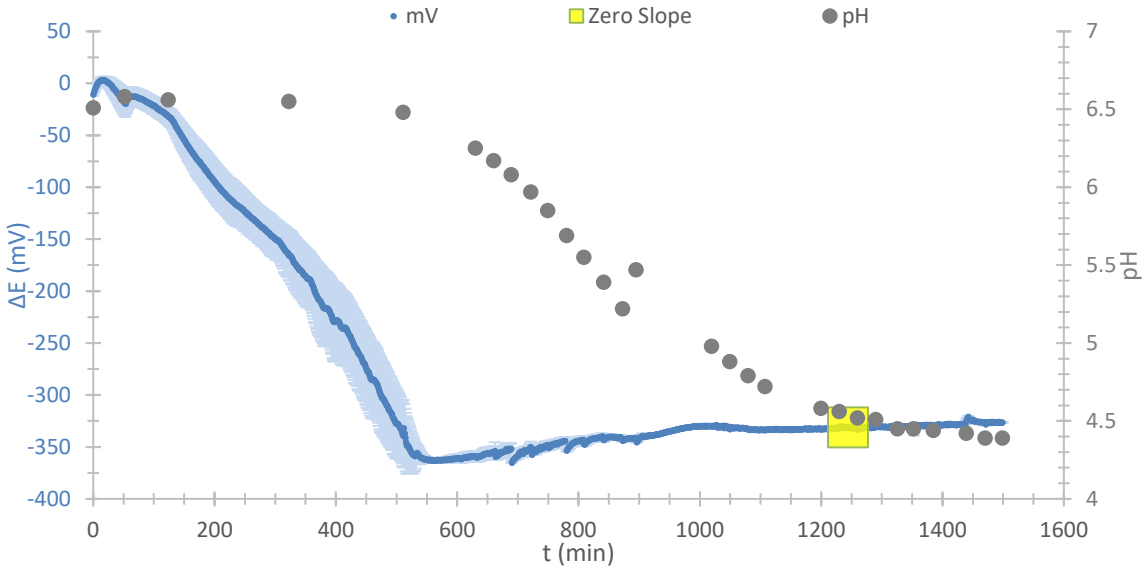

Figure 7. Average MPS Signal (ΔE, mV) and pH using 2.043 g Inoculum Mass. Error bars represent the original two MPS sensor values as minimum and maximum before the average was calculated. The area where the change in energy over 10 minutes was approximately constant (zero slope) is boxed.

Compared Results

Figure 8 illustrates the MPS signal (in mV), and pH values compiled from all four experimental trials with a mass of 2.042 ± 0.001 g. MPS signal and pH values across all experimental trials are seen to follow similar patterns: pH gradually decreasing and

approaching a value near 4.6. MPS signals all slightly increase in a short time period before rapidly decreasing to a minimum value, followed by a gradual increase, stabilization at the isoelectric point, then continuing to slightly increase unpredictably. Depicted in this form, it is clear that the MPS signals follow a progressive set of characteristics, often overlapping and crossing at similar points and with the approximately zero slope area occurring at similar regions.

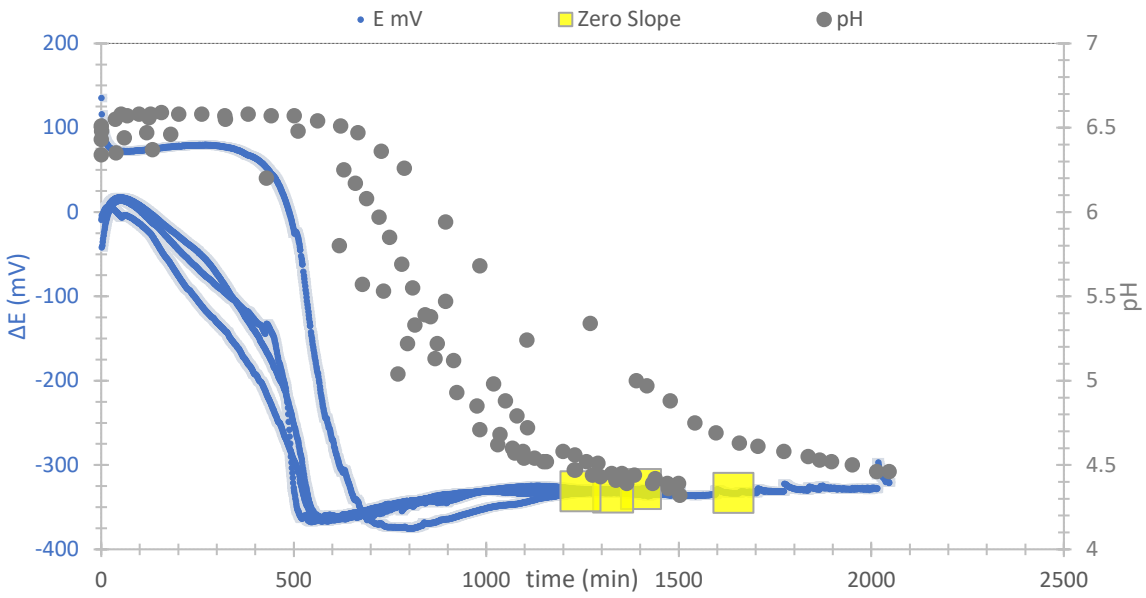

Figure 8. Combined Experimental Data. Error bars represent the two MPS signal (mV) values for each experiment as minimum and maximum values before the average was calculated. The area where the change in energy over 10 minutes was approximately constant (zero slope) is boxed.

Table 1 contains the critical information obtained from each experimental trial. Included is the time of complete fermentation, the slope of MPS signal over time used to

determine this complete fermentation time, the stable MPS signal where fermentation was considered complete, and the pH at this time. Using this information, an average across all trials was calculated to provide the average values of complete fermentation. This results in a pH average of 4.64, which is within the isoelectric range that was expected between 4.0 and 4.7 (de Oliveira, 2014) and well above the targeted pH of 4.3. The stable MPS signal in this range has an average of -329.7 mV, and as seen in Figure 8, across all experiments, MPS signals are most similar in this range.

Table 1. Complete Fermentation Data. Each experimental trial's MPS signal and pH at the isoelectric point, used to consider complete fermentation.

Experiment Mass (g)	Complete Fermentation Time (min)	10-Minute Slope	MPS Signal (mV)	pH
2.041	1402.05	3.03×10^{-6}	-328	4.38
2.042	1330.20	1.51×10^{-5}	-323	4.41
2.041	1641.95	2.61×10^{-4}	-333	4.65
2.043	1244.68	4.54×10^{-6}	-331	4.54
Average	1404.72	7.09×10^{-5}	-331	4.49

With data organized in this manner, the primary analysis of all four experiments then used the mean complete fermentation time, MPS signal, and pH to produce 95% confidence intervals. This information is displayed in Table 2**.** Here, using the time of complete fermentation and the MPS signal and pH at that time for each experiment, an average value across all experiments was calculated. With four observations each for complete fermentation time, MPS signal, and pH, a 95% confidence interval was constructed, with the lower and upper bounds of the interval listed.

Table 2. **Average Complete Fermentation Time Analysis**. The determined time of complete fermentation (in minutes) and the MPS signal (in mV) and pH at that time from each experiment.

Experiment Mass (g)	Complete Fermentation Time (min)	MPS Signal (mV)	pH
2.041	1402.05	-328.6	4.38
2.042	1330.20	-332.9	4.41
2.041	1641.95	-333.2	4.65
2.043	1244.68	-331.3	4.54
Standard Deviation	147.8	1.765	0.266
95% Confidence Interval	165.7	1.978	0.11
Lower Bound	1239.0	-333.4	4.37
Mean	1404.7	-331.4	4.49
Upper Bound	1570.4	-329.4	4.61

In Table 2, the experiment using 2.041 g of inoculum mass and a complete fermentation time of 1641.95 minutes is longer than the other experiments. In this experiment, it took over 200 minutes longer to reach complete fermentation than in the other experiment using 2.041 g of inoculum mass. This longer fermentation time may be a result of multiple factors. First, the moisture content of the inoculum may have affected the suspension of the culture into the milk, altering the initial mixing and proliferation of the yogurt culture. An assumption of complete mixing, however, was acknowledged as a limitation yet may here be seen to have an effect on results. Also, the temperatures of the longer fermentation time ran about 1 ºC lower for the duration of the experiment than in the shorter fermentation time experiment. Again, temperature was acknowledged to be assumed constant, however when acting uniformly for the entire experiment, aggregate

effects may result in a longer fermentation time at a slightly lower fermentation temperature.

Using the intervals displayed in Table 2, it is evident that the duration of time to reach complete fermentation may vary by over two hours. This is an undesirably large range of time that complete fermentation may be reached within, yet using the times from four experiments may be reported with 95% confidence. In contrast, MPS signal is more limited in range, within less than 2 mV above and below the mean MPS signal value. At last, pH results in the smallest variance in range, with the upper confidence around the hypothesized pH target of 4.6. With the upper confidence bound of pH = 4.61, this may be where complete fermentation just begins, and the lower range of pH = 4.37 well into complete fermentation.

Method Detection Limit

The method detection limit was calculated to assess the limit, in this case the minimum amount of time, that may confidently be reported using the prescribed method. Using all four experimental trials, there are four times of complete fermentation used for this MDL calculation. This results in three degrees of freedom and a corresponding Student's t-value of 2.353 for 95% confidence (U.S. EPA, Office of Water, 2016). At last, using the standard deviation in complete fermentation times and this t-value, an MDL of 347.9 minutes was calculated. This may be interpreted as using the currently outlined analytical method of MPS signals used to determine complete fermentation time is confidently accurate down to a minimum of 347.9 minutes. The calculation of the

MDL is organized in Table 4 and displayed as MDL in time versus inoculum mass in Figure 9.

Table 3. Calculation of the Method Detection Limit (MDL). The time of complete fermentation (in minutes) of four observations and the standard deviation of these times were used to calculate the MDL. The statistical values used in the calculation of the MDL are listed.

Experiment Mass (g) and Time (min)	Statistical Values
2.041 : 1402.05	Number of Observations = 4 (df = 3)
2.042 : 1330.20	Confidence Level = 95%
2.041 : 1641.95	Student's t-value = 2.353
2.043 : 1244.68	Standard Deviation = 147.8 (min)
MDL = 347.9 (min)	

Figure 9. Method Detection Limit (MDL) for Time. Time (in minutes) calculated from all four experiments. With an average mass of 2.042 g, vertical error bars of 0.001 g capture the mass of all experiments. Horizontal error bars capture with 95% confidence the MDL using the four experiment's complete fermentation times and resulting standard deviation.

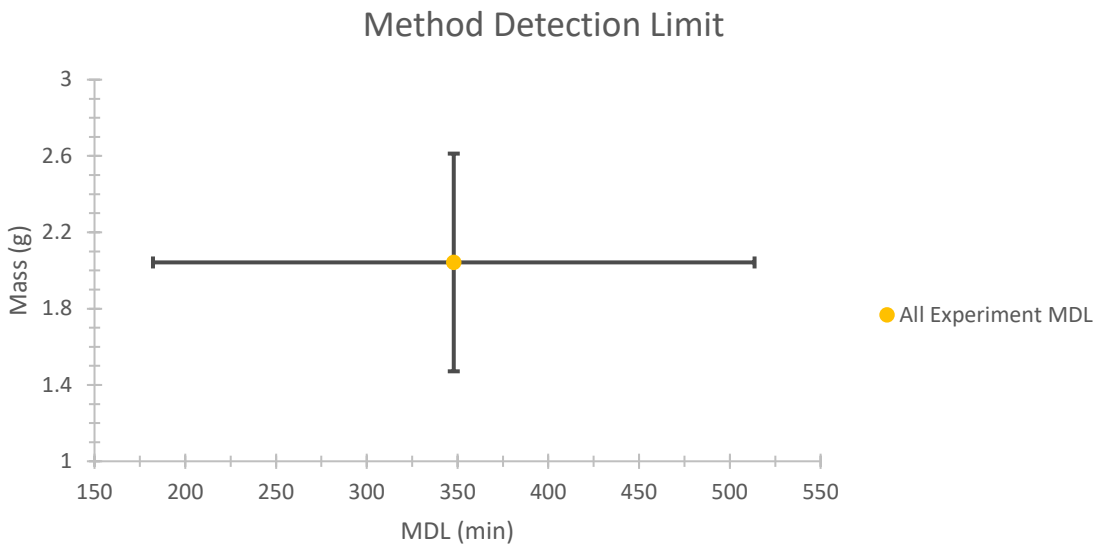

Sensitivity Analysis

First, the data obtained was screened for outliers. As the inoculum mass used in the initial experiment, 0.508 g, was significantly different than the inoculum masses used in the remaining experiments, the first experimental trial was considered an outlier trial. Data from this initial experiment may in turn not be comparable across trials as the data obtained from the other experiments. As such, the sensitivity analysis would exclude this trial to assess the effects of including or excluding these data would have on the results. Similarly, the second experiment's mass of 2.027 g was more than 0.01 grams below the

remaining experiments, this trial was considered an outlier and excluded from further analysis.

The experiments themselves were identified to have naturally occurring groups based on the inoculum mass used. Experiments were grouped into clusters for further sensitivity analysis. The first cluster consists of two experiments which both had the same inoculum mass of exactly 2.041 g, which were then grouped together as a cluster. The next cluster contained the remaining two experiments of 2.042 g and 2.043 g, grouped as an average mass of 2.0425 ± 0.0001 g. All four of these experiments are all within 0.001 grams of 2.042 g, and would be grouped as 2.042 ± 0.001 g. These three cluster groupings were then used in the sensitivity analysis to assess differences when considering grouping by this method.

Using these clusters, a similar analysis was performed to that in the primary analysis and Table 2. The primary analysis results were compared to the cluster analysis in this sensitivity analysis. In the first identified cluster with a mass of 2.041 grams, the same calculation methods were used to obtain the mean, standard deviation, and then 95% confidence interval. The results of this cluster analysis are found in Table 4.

Table 4. First Clustered Complete Fermentation Time Analysis- 2.041 g Inoculum Mass. The determined time of complete fermentation (in minutes) is used with the corresponding MPS signal (in mV) and pH at that time from each experiment.

Inoculum Mass (g)	Complete Fermentation Time (min)	MPS Signal (ΔE, mV)	pH
2.041	1402.05	-328.6	4.38
2.041	1641.95	-333.2	4.64
Standard Deviation	119.95	2.275	0.13
95% Confidence Interval	190.11	3.605	0.21
Lower Bound	1331.8	-334.5	4.30
Mean	1522.00	-330.9	4.51
Upper Bound	1712.11	-327.3	4.72

While using only two experiments results in fewer observations, the resulting confidence intervals from this cluster are different than those calculated in the primary analysis. The time range in complete fermentation time captured with 95% confidence is larger than that of the primary analysis by about 45 minutes. At the same time, the MPS signal and pH confidence intervals are higher than those of the primary analysis, and may be concluded to be less precise in confidently containing the most likely MPS signal and pH value when fermentation is complete despite analyzing the same inoculum mass. With the upper bound of pH = 4.72, this is highly likely before complete fermentation occurs, yet the mean and lower bound well below the hypothesized pH target of 4.6. These large confidence intervals are potentially the result of limited observations that all are relatively distinct, rather than closely similar values as hypothesized. This is evidenced in the upper bound of pH = 4.72, well above the pH where the yogurt mixture

is completely fermented, with predictions of complete fermentation that would be premature.

The next cluster investigated contained an average inoculum mass of 2.0425 ± 0.0001 grams. The same method used in the previous cluster and in the primary analysis for all experiments was followed. The result of analyzing by this cluster is presented in Table 5.

Table 5. Second Clustered Complete Fermentation Time Analysis- 2.0425 ± 0.0001 g Inoculum Mass. The determined time of complete fermentation (in minutes) is used with the corresponding MPS signal (in mV) and pH at that time from each experiment.

Inoculum Mass (g)	Complete Fermentation Time (min)	MPS Signal (mV)	pH
2.042	1330.2	-332.7	4.410
2.043	1244.6	-331.35	4.54
Standard Deviation	42.758	0.675	0.065
95% Confidence Interval	67.76	1.06	0.10
Lower Bound	1219.6	-333.0	4.37
Mean	1287.4	-332.0	4.47
Upper Bound	1355.2	-330.9	4.57

Analysis of this second cluster has the same number of observations as the previous cluster, yet yields different results. By analyzing this cluster, the confidence interval for time of complete fermentation decreases in range to about a third the time of the previous cluster, remaining smaller than that of the primary analysis at just over an hour range. The confidence interval for MPS signal and pH are smaller than in the previous cluster analysis. All pH values are below the pH target of 4.6, and this range

may be inferred to most confidently contain the pH of complete fermentation. With these results, it may be reported that this average and 95% confidence interval construction method is fairly robust across these analyzed clusters. While the variance in time range that may confidently be reported to contain the time of complete fermentation is reduced to approximately one hour long, the significantly different results between clusters informs analysis of similar, but limited, experiments bring more stringent results using this sensitivity analysis method.

To assess the robustness of the results of determining an exact time of complete fermentation, 10-minute ranges were constructed for each experiment. This range would center around the previously determined time as complete fermentation, with approximately five minutes before and five minutes after to provide a time range. This redefined threshold was used to assess the sensitivity of selecting an individual time considered to be complete fermentation that may vary within the range. With these ranges constructed identically for each experiment, the confidence in using the same MPS signal analysis methodology to determine the complete fermentation time may be compared more directly across experimental trials. When clustering these 10-minute ranges, this also presents more data that may be analyzed than used in the primary analysis, which may lead to more accurate results.

The critical information of these 10-minute ranges is included in Table 6. The time, MPS signal, and pH values at the start and end of each experiment's range is included, with the complete time as previously determined and used in the primary analysis. Next, the mean of the values contained in the 10-minute range is listed. Because

the range consists of the same time span for each trial, the standard deviations of time, MPS signal, and pH were approximately the same between trials and are excluded from this table. From here, a 95% confidence interval may be constructed, with the lower and upper bounds provided based on the data set. With this level of confidence and using 10 minutes of data, this results in capturing the complete fermentation time and that time's MPS signal and pH within five minutes and 95% confidence. This is a greater accuracy of confidence in each experimental trial than that of the primary analysis. Each experiment's 10-minute range represents less than 1% of the entire experiment's data; this limits the experiment's complete data to be bound by the time area of interest where complete fermentation is most likely captured and reduces variance. Further, the mean values of time, MPS signal, and pH as calculated from the complete data contained in the 10-minute range are very close to the previously considered timestamp values of complete fermentation as in the primary analysis. Using 10 data points rather than one for each trial results in a more representative complete fermentation time, and the MPS signal and pH value at this point than used in the primary analysis.

Table 6. Complete Fermentation Ranges. The beginning of the time range is five minutes before the previously determined complete fermentation time, and end of the range five minutes after. The percentage of time this 10-minute range represents is included. The MPS signal and pH at all times is listed. Lower and upper confidence interval bounds are included for 95% confidence about the mean of the entire 10-minute range of values.

Experiment and Mass (Range Percentage)	Target	Time (min)	MPS Signal (mV)	pH
3: 2.041 g (0.66%)	Range Start	1397.4	-328.8	4.38
	Complete Time	1402.0	-328.6	4.38
	Range End	1407.8	-328.6	4.38
	Lower Bound	1400.1	-328.7	4.38
	Mean	1402.6	-328.6	4.38
	Upper Bound	1405.1	-328.6	4.38
4: 2.042 g (0.70%)	Range Start	1326.7	-332.8	4.41
	Complete Time	1330.2	-332.7	4.41
	Range End	1337.1	-332.9	4.40
	Lower Bound	1328.2	-333.0	4.40
	Mean	1330.7	-332.9	4.41
	Upper Bound	1645.0	-333.1	4.64
11: 2.041 g (0.49%)	Range Start	1637.3	-333.2	4.65
	Complete Time	1641.9	-333.2	4.64
	Range End	1647.7	-333.2	4.63
	Lower Bound	1640.0	-333.2	4.64
	Mean	1642.5	-333.2	4.64
	Upper Bound	1645.0	-333.1	4.64
12: 2.043 g (0.67%)	Range Start	1240.0	-331.4	4.54
	Complete Time	1244.6	-331.3	4.54
	Range End	1250.4	-331.4	4.53
	Lower Bound	1242.7	-331.5	4.53
	Mean	1245.2	-331.4	4.53
	Upper Bound	1247.7	-331.3	4.54

With the 10-minute ranges organized, the previously described clusters were be examined. To directly compare the ranges, each experiment's 10-minute range was transformed using a standard distribution, setting the mean as the originally determined time of complete fermentation and standard deviation of one. The data contained in each 10-minute range was converted into a Z-score using these mean and standard deviation values allowing data to be compared across ranges. Z-scores were then reverted to time, MPS signal, and pH values using the original mean and standard deviation of the combined data set.

To assess the use of these time ranges to calculate confidence intervals, the same clustering of experiments was used. First, the cluster with experiments of the same mass 2.041 g was assembled using the standardized Z-scores. This range now has 20 observations. The mean Z-score for complete fermentation time, MPS signal, and pH was then calculated. 95% confidence intervals for complete fermentation time, MPS signal, and pH were then constructed using the Z-scores before these values were reverted to the corresponding original unit. Results of analyzing the first cluster are displayed in Table 7.

Table 7. First Clustered Complete Fermentation Time Range Analysis- 2.041 g Inoculum Mass. The 10-minute range for complete fermentation (in minutes) and the corresponding MPS signal (in mV) and pH at that time from each experiment's 10-minute time range. The 95% confidence interval lower and upper bounds are listed for each value. Using two 10-minute ranges, 20 total observations are used in this cluster.

2.041 g N = 20	Complete Fermentation Time (min)	MPS Signal (mV)	pH
Lower Bound	1482.9	-333.0	4.41
Mean	1522.0	-330.9	4.51
Upper Bound	1603.1	-331.0	4.55
Range	120.2	2.0	0.14

Analysis of this first cluster results in the smallest confidence interval range for MPS signal. Interestingly, the time range of the upper and lower bounds of the 95% confidence interval is approximately the same as the standard deviation obtained by analyzing complete fermentation as a single time point. This lends support to the confidence in this result as via both a time range and single time point method to calculate this interval, a relatively similar time range results.

The second cluster containing with an average inoculum mass of 2.0425 grams and a standard deviation of 0.0001 grams was analyzed in the same manner. The results of this cluster analysis are presented in Table 8.

Table 8. Second Clustered Complete Fermentation Time Range Analysis- 2.0425 ± 0.0001 g Inoculum Mass. The 10-minute range for complete fermentation (in minutes) and the corresponding MPS signal (in mV) and pH at that time from each experiment's 10-minute time range. The 95% confidence interval lower and upper bounds are listed for each value. Using two 10-minute ranges, 20 total observations are used in this cluster.

2.0425 ± 0.0001 g N = 20	Complete Fermentation Time (min)	MPS Signal (mV)	pH
Lower Bound	1273.4	-333.1	4.43
Mean	1287.4	-332.0	4.47
Upper Bound	1316.3	-331.5	4.50
Range	42.9	1.6	0.07

Analysis of the second cluster containing 20 observations results in the smallest range in the confidence interval for complete fermentation time and is less than one hour in range. While the entire range of pH is below 4.6 as expected for complete fermentation, this pH range is the half that of the first; this garners support that this analytical method is more stringent as more precise results are produced when similar but not identical experimental inoculum masses are analyzed by cluster.

The third cluster containing all four experiments with an average inoculum mass of 2.042 grams and a standard deviation of 0.001 grams was analyzed in the same manner. The results of this cluster analysis are presented in Table 9.

Table 9. All Experiments Clustered Complete Fermentation Time Range Analysis-2.042 ± 0.001 g Inoculum Mass. The 10-minute range for complete fermentation (in minutes) and the corresponding MPS signal (in mV) and pH at that time from each experiment's 10-minute time range. The 95% confidence interval lower and upper bounds are listed for each value. Using all four 10-minute ranges, 40 total observations are used in this cluster.

2.042 ± 0.001 g N = 40	Complete Fermentation Time (min)	MPS Signal (mV)	pH
Lower Bound	1378.2	-333.5	4.44
Mean	1404.7	-331.4	4.49
Upper Bound	1482.0	-330.6	4.51
Range	103.8	2.9	0.07

Analysis of the third cluster containing all four experiments and 40 observations results in a confidence interval for complete fermentation time slightly larger than the second cluster yet smaller than that of the first cluster analysis. The pH range for this cluster is the same as the previous cluster, suggesting this is a robust result and the pH of complete fermentation is indeed contained within 0.07 pH-points.

CHAPTER 5

CONCLUSION

Research Advancement

This study tested the ability of MPS to produce signals in a medium that was not previously evaluated. Using the same system tools and analytical methods as previous developments of MPS technology, this research serves as a proof-of-concept investigation (Thabane et al., 2010) of using MPS technology to monitor a model yogurt fermentation process. Processing conditions mimicked those of commercial yogurt production. Under these conditions, measurable and quantifiable information was obtained. The multimetric data continuously collected by the MPS technology in this yogurt medium validates the simple-to-use feasibility of the technology and supports future developments of this technology similarly in additional mediums.

The MPS technology produced signals as hypothesized, allowing for analytical methods to predict the time where fermentation of the yogurt is complete. However, a challenge remains in refining the accuracy of the predicted complete fermentation time. A desirable five minute range which contains the time fermentation is complete was hypothesized to be feasibly predicted by the analytical method; yet this current hypothesis is not supported by the results reached in this study. While progress toward this desired goal was made, over a one-hour window of accuracy remains.

A systematic literature review informed the progress and remaining challenges of applying MPS and similar sensor technologies to a variety of mediums, including food products that undergo fermentation reactions. This literature review advised the

anticipated relationships between pH, oxidation-reduction states, temperature, and microbial biofilm that underpin the MPS technology and the desired operation of MPS in yogurt fermentation. These relationships were then observed in a series of experiments which produced insightful quantified data. Data was then analyzed through previous methods to assess the abilities and remaining difficulties in adapting MPS technology in this new medium.

As hypothesized, and supported in previous literature, the isoelectric range of the yogurt fermentation mixture was observed to be reached around a pH of 4.6. Data was captured continuously during this range, which further aided in the selection of complete fermentation times. The MPS technology, by continuously recording beyond this range, successfully captured the natural degradation of the completely fermented yogurt product. This untargeted success doubles as a food product safety test, as detection of MPS signal activity beyond the time of complete fermentation indicates bacterial colonization or contamination which must be avoided (de Oliveira, 2014) at larger production scales.

Despite the different bacterial inoculum masses used to ferment the staring dairy material to yogurt product, MPS signals were captured. These signals followed similar and predictable patterns which could all be used to predict the complete fermentation time of the mixture. Even administering the same inoculum dose in different experimental trials, the complete fermentation times were not the same; further, simple correlative analysis indicates the relationship between inoculum mass and the time to reach complete fermentation is not a strong linear relationship as it was expected to

produce. As the fermentation end time varied despite using the same dose, it was concluded as supported by the obtained results that this metric is not as reliable as anticipated in this study.

By determining the MDL, the analytical method's limitations in determining the times of complete fermentation are indicated to not be as low and precise as desired. Yet through alternative reanalysis using this study's sensitivity analysis, the MDL remains fairly robust; providing confidence that the current method of determining the complete fermentation time is valid despite resulting in an undesirably high MDL (U.S. EPA, Office of Water, 2016).

Reflections

Reassessment by the sensitivity analysis performed in this study allows for examination of the analytical method's effectiveness (Thabane et al., 2013). In most cases, the sensitivity analysis included more comprehensive analysis and calculated more stringent results, whereas the primary analysis quickly revealed more relaxed results for further interpretation. The sensitivity analysis determined a method of clustering time ranges from each experiment with similar, but not exactly the same, inoculum masses rendered the most precise results. This method used in the sensitivity analysis pruned the variance of predicted complete fermentation times from about two hours to around 45 minutes. While this range remains undesirably large, this method may be identified as a preferred analytical method for obtaining a more stringent resulting timeframe.

At the same time, MPS signal and pH reanalysis in the sensitivity analysis were found to remain relatively similar to the results of the primary analysis, supporting the simple primary analysis to be a robust method of predicting these values at the complete fermentation time. Similarly, results of correlating inoculum mass and complete fermentation time were nearly the same in both the primary analysis and the sensitivity analysis. This indicates the method of correlating these two values is very robust, despite a moderate degree of linear correlation as supported by the obtained data.

The sensitivity analysis most importantly reveals that analyzing data in clusters centered around similar, but not exactly the same, inoculum mass produces results with the smallest confidence interval ranges. This modulation of data is more restrictive, yet incorporates more data than would be included in using the exact same inoculum mass. From this conclusion, it may be inferred that a greater quantity of data that is centered closely around the identified clustering, here inoculum mass, presents the results that may be more confidently interpreted as precise.

The limitations of this study must be once again discussed for consideration. While temperature was assumed to be approximately constant, and monitoring confirmed temperatures remained within a 3 ºC range while culturing, variance within this range was recorded. As previously reported, a 10 ºC optimal temperature range exists (Ahari et al., 2017), and while well within this range, an incubator would provide consistent and constant temperatures. In industrial settings, temperature is similarly consistent and constant. Temperature is importantly related to microbial activity, pH, and reaction kinetics (Burge et al., 2020). Another limitation is the assumption of complete mixing of

the culture into the staring milk material. While in an industrial setting an inoculum would be thoroughly blended, at the bench scale of this project, mixing was sufficient. Continually mixing was not continued as the yogurt was cultured, which is a consideration of reaction kinetics. Nonetheless, the culturing method used remains a viable yogurt production method (de Oliveira, 2014) as a set yogurt rather than stirred. Additionally, the cultures used in this method were not pure cultures, and no work was performed to quantify and ensure their viability. While yogurt was successfully produced, it is likely the inoculum cultures were viable; in any case, biofilm was able to develop on the MPS surface and produce signals of use. Given these limitations, they may be negligible at this bench scale as a method to assess the feasibility of the MPS technology and following analytical methods.

Interpreting the results of this study focuses on the feasibility of utilizing MPS technology in this previously untested medium and the quality of the results produced as assessed and compared using a sensitivity analysis. Despite recurrent imprecisions, MPS successfully produced signals which resulted in data rich in information. In this small study, multiplicity challenges were faced as repeated identical experimental treatments resulted in multiple outcomes. However, as this work incorporates natural biological components and given the conditions and assumptions, this is acceptable. This multiplicity should not prevent further work in developing MPS technology yet rather proposes additional testing. Analytical methods were adapted and work remains to further optimize these methods to have greater sensitivity. Greater sensitivity, as indicated by a lower MDL, would promote the MPS technology to further applications and larger scales.

Even at the undesirable levels of precision in this work, MPS technology again successfully demonstrated the ability to monitor reaction progress in continuous real-time; this remains valuable to identify undesired microbial contamination, natural product decomposition, and the associated losses of time, materials, and productivity that would result from these production issues.

Recommendations

Despite the limitations and considerations of this study, performance of MPS as hypothesized and in support of the research objectives demonstrates the facile deployment of the technology and readiness for this technology to be applied to additional settings. As such, future research of MPS technology may be recommended. Additional work may seek to confirm the results of this study; further research may also build upon additional analytical methods to interpret the data obtained from MPS. Most importantly, the completion of additional experimental trials would provide additional data that may further refine the methods and bring more desirable results. This study completed six experiments; to reach a method that may predict complete fermentation time within five minutes with 95% confidence and the same standard deviation observed in this work, it is calculated that 4,900 experiments would be needed to obtain the number of complete fermentation times to obtain this goal. While this is an obvious estimate and does not account for a potentially smaller standard deviation resulting from this many trials, this is an unrealistic task; nonetheless, additional trials would obtain a more comprehensive perspective of the targeted relationships to be analyzed.

In performing additional experiments, the use of different inoculum masses would set up for more comprehensive correlations between inoculum mass and time for complete fermentation. This study utilized the inoculum masses near the minimum ratios as recommended (de Oliveira, 2014), however, incrementing inoculum masses linearly between 0.5 grams through 5.0 grams would allow for additional correlation points. Using this, a standard curve may be developed and serve as a calibration proof of concept in this setting.

This study did not include a blank, control experimental trial. While the MPS technology uses microbial biofilm on the sensor's surface for measurements, understanding a baseline condition in the absence of the inoculating bacteria may also be of benefit in future research.

The repeatable patterns obtained in this research lend well to machine learning and artificial intelligence. These advanced computational modeling methods, when trained with an appropriate amount of data, offer far greater precision in predicting complete fermentation times using inoculum mass, MPS signal, and pH value variables. Alternatively, greater precision in predictive power may be reached by adjusting the level of confidence in conjunction with compiling additional data.

Field Contributions

Finally, previous advances in sensing technologies and the current state of MPS technology were reviewed. A gap was identified where food safety is at risk from decomposition or lost productivity, as well as the inability to expose food products to

reagents or contamination as in other sensing approaches that may diffuse internal solutions. MPS was prepared for testing in a new application, accomplishing similar feasibilities as in previous demonstrations: generation of signal outputs, no maintenance, continuous and real-time monitoring data, no additional reagents, and ease of use. This feasibility further prompts MPS technology for further investigation in this capacity as well as for deployment in new settings and environments.

The underlying theory of the MPS technology's operation was validated in this study. Biofilm covered the sensor surfaces, interacting with the conditions of the yogurt medium as it undergoes a redox fermentation process. These interactions and changes in bioactivity were measurable and recorded by the MPS, producing insightful data. With this demonstrated success, further applications where these reactions are present may investigated by using MPS monitoring. Fermentation processes occurs for the production of many food products: soy products including soy sauce and tempeh, coffee beans, beer, wine, kombucha, vinegars, other dairy products (Winquist et al., 1998) including cheeses (Casimero et al., 2018; Chinnathambi & Euverink, 2019; Draz et al., 2021), and pickled vegetables.

Outside the range of food products, redox processes may be further monitored by MPS technology. In health, many applications are possible for similar deployment: electrochemical detection of viral elements in blood (B. T. T. Nguyen et al., 2009), bacterial infections of clinical importance (Poma et al., 2020; Wu et al., 2015), noninvasive cell monitoring (Reinecke et al., 2017), and many types of bioreactors (O'Mara et al., 2018). Further, starch and vegetable sugars are fermented to produce fuel

ethanol, a biofuel alternative to traditional fossil fuels (Ramos et al., 2016). Even beyond, as 95% of microbes form biofilms (Flemming et al., 2002), the applicability of the technology is expansive in many environmental contexts.

REFERENCES

40 CFR § 141.74—Analytical and monitoring requirements. Retrieved November 3, 2021, from https://www.law.cornell.edu/cfr/text/40/141.74

Abokifa, A. A., Yang, Y. J., Lo, C. S., & Biswas, P. (2016). Water quality modeling in the dead end sections of drinking water distribution networks. *Water Research*, *89*, 107–117. https://doi.org/10.1016/j.watres.2015.11.025

Ahari, H., Hedayati, M., Akbari-adergani, B., Kakoolaki, S., Hosseini, H., & Anvar, A. (2017). *Staphylococcus aureus* exotoxin detection using potentiometric nanobiosensor for microbial electrode approach with the effects of pH and temperature. *International Journal of Food Properties*, 1–10. https://doi.org/10.1080/10942912.2017.1347944

Allaire, M., Wu, H., & Lall, U. (2018). National trends in drinking water quality violations. *Proceedings of the National Academy of Sciences*, *115*(9), 2078–2083. https://doi.org/10.1073/pnas.1719805115

Ambrosi, A., Chua, C. K., Bonanni, A., & Pumera, M. (2014). Electrochemistry of Graphene and Related Materials. *Chemical Reviews*, *114*(14), 7150–7188. https://doi.org/10.1021/cr500023c

American Chlorine Chemistry Council. (2003). *Drinking Water Chlorination: A Review of Disinfection Practices and Issues*. https://waterandhealth.org/safe-drinking-water/wp/

Azeredo, J., Azevedo, N. F., Briandet, R., Cerca, N., Coenye, T., Costa, A. R., Desvaux, M., Di Bonaventura, G., Hébraud, M., Jaglic, Z., Kačániová, M., Knøchel, S., Lourenço, A., Mergulhão, F., Meyer, R. L., Nychas, G., Simões, M., Tresse, O., & Sternberg, C. (2017). Critical review on biofilm methods. *Critical Reviews in Microbiology*, *43*(3), 313–351. https://doi.org/10.1080/1040841X.2016.1208146

Azzarelli, J. M., Mirica, K. A., Ravnsbæk, J. B., & Swager, T. M. (2014). Wireless gas detection with a smartphone via rf communication. *Proceedings of the National Academy of Sciences*, *111*(51), 18162–18166. https://doi.org/10.1073/pnas.1415403111

Bagotsky, V. S. (2005). Aqueous Electrolyte Solutions. In *Fundamentals of Electrochemistry* (pp. 99–126). John Wiley & Sons, Ltd. https://doi.org/10.1002/047174199X.ch7

Bai, X., Ma, X., Xu, F., Li, J., Zhang, H., & Xiao, X. (2015). The drinking water treatment process as a potential source of affecting the bacterial antibiotic

resistance. *Science of The Total Environment*, *533*, 24–31. https://doi.org/10.1016/j.scitotenv.2015.06.082

Bai, Z., Li, G., Liang, J., Su, J., Zhang, Y., Chen, H., Huang, Y., Sui, W., & Zhao, Y. (2016). Non-enzymatic electrochemical biosensor based on Pt NPs/RGO-CS-Fc nano-hybrids for the detection of hydrogen peroxide in living cells. *Biosensors and Bioelectronics*, *82*, 185–194. https://doi.org/10.1016/j.bios.2016.04.004

Bao, H., Zheng, Z., Yang, B., Liu, D., Li, F., Zhang, X., Li, Z., & Lei, L. (2016). In situ monitoring of Shewanella oneidensis MR-1 biofilm growth on gold electrodes by using a Pt microelectrode. *Bioelectrochemistry*, *109*, 95–100. https://doi.org/10.1016/j.bioelechem.2016.01.008

Bard, A. J., & Faulkner, L. R. (2001). Potential sweep methods. *Potential Sweep Methods*, 226–260.

Bard, L. R., & Faulkner. (2001). Introduction and Overview of Electrode Processes. *A. J. & Faulkner, John Wiley & Sons, Editor*, *2*, 1.

Bause, S., Decker, M., Gerlach, F., Näther, J., Köster, F., Neubauer, P., & Vonau, W. (2018). Development of an iridium-based pH sensor for bioanalytical applications. *Journal of Solid State Electrochemistry*, *22*(1), 51–60. https://doi.org/10.1007/s10008-017-3721-1

Bhat, S. A., Cui, G., Li, W., Wei, Y., & Li, F. (2020). Effect of heavy metals on the performance and bacterial profiles of activated sludge in a semi-continuous reactor. *Chemosphere*, *241*, 125035. https://doi.org/10.1016/j.chemosphere.2019.125035

Bimakr, F., Ginige, M. P., Kaksonen, A. H., Sutton, D. C., Puzon, G. J., & Cheng, K. Y. (2018). Assessing graphite and stainless-steel for electrochemical sensing of biofilm growth in chlorinated drinking water systems. *Sensors and Actuators B: Chemical*, *277*, 526–534. https://doi.org/10.1016/j.snb.2018.09.005

Blaen, P. J., Khamis, K., Lloyd, C. E. M., Bradley, C., Hannah, D., & Krause, S. (2016). Real-time monitoring of nutrients and dissolved organic matter in rivers: Capturing event dynamics, technological opportunities and future directions. *Science of The Total Environment*, *569–570*, 647–660. https://doi.org/10.1016/j.scitotenv.2016.06.116

Bohrerova, Z., Stralkova, R., Podesvova, J., Bohrer, G., & Pokorny, E. (2004). The relationship between redox potential and nitrification under different sequences of crop rotations. *Soil and Tillage Research*, *77*(1), 25–33. https://doi.org/10.1016/j.still.2003.10.006

Bonanni, P. S., Schrott, G. D., Robuschi, L., & Busalmen, J. P. (2012). Charge accumulation and electron transfer kinetics in Geobacter sulfurreducens biofilms. *Energy & Environmental Science*, *5*(3), 6188. https://doi.org/10.1039/c2ee02672d

Bond, D. R., & Lovley, D. R. (2003). Electricity Production by *Geobacter sulfurreducens* Attached to Electrodes. *Applied and Environmental Microbiology*, *69*(3), 1548–1555. https://doi.org/10.1128/AEM.69.3.1548-1555.2003

Bourrie, B. C. T., Willing, B. P., & Cotter, P. D. (2016). The Microbiota and Health Promoting Characteristics of the Fermented Beverage Kefir. *Frontiers in Microbiology*, *7*. https://doi.org/10.3389/fmicb.2016.00647

Bowler, P. G. (2003). The 10(5) bacterial growth guideline: Reassessing its clinical relevance in wound healing. *Ostomy/Wound Management*, *49*(1), 44–53.

Brastad, K. S., & He, Z. (2013). Water softening using microbial desalination cell technology. *Desalination*, *309*, 32–37. https://doi.org/10.1016/j.desal.2012.09.015

Britton, H. T. S., & Robinson, R. A. (1931). CXCVIII.—Universal buffer solutions and the dissociation constant of veronal. *J. Chem. Soc.*, *0*(0), 1456–1462. https://doi.org/10.1039/JR9310001456

Brown, F. C., Burge, S. R., Hristovski, K. D., Burge, R. G., Taylor, E., & Hoffman, D. A. (2020). Microbial potentiometric sensor technology for real-time detecting and monitoring of toxic metals in aquatic matrices. *Macedonian Journal of Chemistry and Chemical Engineering*, *39*(2), 119. https://doi.org/10.20450/mjcce.2020.2088

Buchenauer, A., Hofmann, M. C., Funke, M., Büchs, J., Mokwa, W., & Schnakenberg, U. (2009). Micro-bioreactors for fed-batch fermentations with integrated online monitoring and microfluidic devices. *Biosensors and Bioelectronics*, *24*(5), 1411–1416. https://doi.org/10.1016/j.bios.2008.08.043

Burge, S. R., Hoffman, D. A., Burge, S. R., & Hoffman, D. A. (n.d.). *MONITORING AND IMAGING OF AN ENVIRONMENT*. 18.

Burge, S. R., Hoffman, D. A., Burge, S. R., & Hoffman, D. A. (2019). *MONITORING AND IMAGING OF AN ENVIRONMENT* (Patent No. US 2019/0107509 Al).

Burge, S. R., Hristovski, K. D., Burge, R. G., Hoffman, D. A., Saboe, D., Chao, P., Taylor, E., & Koenigsberg, S. S. (2020). Microbial potentiometric sensor: A new approach to longstanding challenges. *Science of The Total Environment*, *742*, 140528. https://doi.org/10.1016/j.scitotenv.2020.140528

Burge, S. R., Hristovski, K. D., Burge, R. G., Saboe, D., Hoffman, D. A., & Koenigsberg, S. S. (2021). Microbial potentiometric sensor array measurements in unsaturated soils. *Science of The Total Environment*, *751*, 142342. https://doi.org/10.1016/j.scitotenv.2020.142342

Cai, H., & Wang, P. (2010). *Mechanisms of Cell-Based Biosensors*. 28.

Casimero, C., McConville, A., Fearon, J.-J., Lawrence, C. L., Taylor, C. M., Smith, R. B., & Davis, J. (2018). Sensor systems for bacterial reactors: A new flavin-phenol composite film for the in situ voltammetric measurement of pH. *Analytica Chimica Acta*, *1027*, 1–8. https://doi.org/10.1016/j.aca.2018.04.053

Chadwick, G. L., Jiménez Otero, F., Gralnick, J. A., Bond, D. R., & Orphan, V. J. (2019). NanoSIMS imaging reveals metabolic stratification within current-producing biofilms. *Proceedings of the National Academy of Sciences*, *116*(41), 20716–20724. https://doi.org/10.1073/pnas.1912498116

Chinnathambi, S., & Euverink, G.-J. (2019). Manufacturing of a Nafion-coated, Reduced Graphene Oxide/Polyaniline Chemiresistive Sensor to Monitor pH in Real-time During Microbial Fermentation. *Journal of Visualized Experiments*, *143*, 58422. https://doi.org/10.3791/58422

Cuhel, R. L., Ortner, P. B., & Lean, D. R. S. (1984). Night synthesis of protein by algae1: Algal night synthesis. *Limnology and Oceanography*, *29*(4), 731–744. https://doi.org/10.4319/lo.1984.29.4.0731

Dantism, S., Röhlen, D., Wagner, T., Wagner, P., & Schöning, M. J. (2019). A LAPS-Based Differential Sensor for Parallelized Metabolism Monitoring of Various Bacteria. *Sensors*, *19*(21), 4692. https://doi.org/10.3390/s19214692

de Oliveira, M. N. (2014). FERMENTED MILKS | Fermented Milks and Yogurt. In *Encyclopedia of Food Microbiology* (pp. 908–922). Elsevier. https://doi.org/10.1016/B978-0-12-384730-0.00121-X

Devanthi, P. V. P., & Gkatzionis, K. (2019). Soy sauce fermentation: Microorganisms, aroma formation, and process modification. *Food Research International*, *120*, 364–374. https://doi.org/10.1016/j.foodres.2019.03.010

Dhall, P., Kumar, A., Joshi, A., Saxsena, T. K., Manoharan, A., Makhijani, S. D., & Kumar, R. (2008). Quick and reliable estimation of BOD load of beverage industrial wastewater by developing BOD biosensor. *Sensors and Actuators B: Chemical*, *133*(2), 478–483. https://doi.org/10.1016/j.snb.2008.03.010

Di Natale, C., Macagnano, A., Davide, F., D'Amico, A., Legin, A., Vlasov, Y., Rudnitskaya, A., & Selezenev, B. (1997). Multicomponent analysis on polluted waters by means of an electronic tongue. *Sensors and Actuators B: Chemical*, *44*(1–3), 423–428. https://doi.org/10.1016/S0925-4005(97)00169-X

Domenech, E., Amorós, J. A., & Escriche, I. (2013). Effectiveness of Prerequisites and the HACCP Plan in the Control of Microbial Contamination in Ice Cream and Cheese Companies. *Foodborne Pathogens and Disease*, *10*(3), 222–228. https://doi.org/10.1089/fpd.2012.1305

Donlan, R. (2001). Biofilms and Device-Associated Infections. *Emerging Infectious Diseases*, *7*(2), 277–281. https://doi.org/10.3201/eid0702.010226

Dowley, A., Fitzpatrick, R., Class, A., & Besz, W. (1998). *Measurement of redox potential (Eh) in periodically waterlogged viticultural soils*. *35*, 9.

Draz, M. E., Darwish, H. W., Darwish, I. A., & Saad, A. S. (2021). Solid-state potentiometric sensor for the rapid assay of the biologically active biogenic amine (tyramine) as a marker of food spoilage. *Food Chemistry*, *346*, 128911. https://doi.org/10.1016/j.foodchem.2020.128911

Du, Z., Li, H., & Gu, T. (2007). A state of the art review on microbial fuel cells: A promising technology for wastewater treatment and bioenergy. *Biotechnology Advances*, *25*(5), 464–482. https://doi.org/10.1016/j.biotechadv.2007.05.004

Dunne, W. M. (2002). Bacterial Adhesion: Seen Any Good Biofilms Lately? *Clinical Microbiology Reviews*, *15*(2), 155–166. https://doi.org/10.1128/CMR.15.2.155-166.2002

Eftekhari-Sis, B., Karaminejad, S., & Karimi, F. (2016). A Nano-Biosensor for the Detection of 185delAG Mutation in *BRCA1* Gene, Leading to Breast Cancer. *Cancer Investigation*, *34*(9), 431–439. https://doi.org/10.1080/07357907.2016.1227444

Eggins, B. R. (Ed.). (2002). *Analytical Techniques in the Sciences*. John Wiley & Sons, Ltd. https://doi.org/10.1002/9780470511305

Esteve-Núñez, A., Sosnik, J., Visconti, P., & Lovley, D. R. (2008). Fluorescent properties of c-type cytochromes reveal their potential role as an extracytoplasmic electron sink in Geobacter sulfurreducens. *Environmental Microbiology*, *10*(2), 497–505. https://doi.org/10.1111/j.1462-2920.2007.01470.x

FAO. (2018). *Standard for Fermented Milks*. https://www.fao.org/fao-who-codexalimentarius/codex-texts/list-standards/en/

Favre, M.-F., Carrard, D., Ducommun, R., & Fischer, F. (2009). Online monitoring of yeast cultivation using a fuel-cell-type activity sensor. *Journal of Industrial Microbiology & Biotechnology*, *36*(10), 1307–1314. https://doi.org/10.1007/s10295-009-0614-z

Fiedler, S. (2000). In Situ Long-Term-Measurement of Redox Potential in Redoximorphic Soils. In J. Schüring, H. D. Schulz, W. R. Fischer, J. Böttcher, & W. H. M. Duijnisveld (Eds.), *Redox* (pp. 81–94). Springer Berlin Heidelberg. https://doi.org/10.1007/978-3-662-04080-5_7

Fiedler, S., Vepraskas, M. J., & Richardson, J. L. (2007). Soil Redox Potential: Importance, Field Measurements, and Observations. In *Advances in Agronomy* (Vol. 94, pp. 1–54). Elsevier. https://doi.org/10.1016/S0065-2113(06)94001-2

Fiorda, F. A., de Melo Pereira, G. V., Thomaz-Soccol, V., Rakshit, S. K., Pagnoncelli, M. G. B., Vandenberghe, L. P. de S., & Soccol, C. R. (2017). Microbiological, biochemical, and functional aspects of sugary kefir fermentation—A review. *Food Microbiology*, *66*, 86–95. https://doi.org/10.1016/j.fm.2017.04.004

Fish, K. E., & Boxall, J. B. (2018). Biofilm Microbiome (Re)Growth Dynamics in Drinking Water Distribution Systems Are Impacted by Chlorine Concentration. *Frontiers in Microbiology*, *9*, 2519. https://doi.org/10.3389/fmicb.2018.02519

Flemming, H.-C., Percival, S. L., & Walker, J. T. (2002). Contamination potential of biofilms in water distribution systems. *Water Supply*, *2*(1), 271–280. https://doi.org/10.2166/ws.2002.0032

Flemming, H.-C., Wingender, J., Szewzyk, U., Steinberg, P., Rice, S. A., & Kjelleberg, S. (2016). Biofilms: An emergent form of bacterial life. *Nature Reviews Microbiology*, *14*(9), 563–575. https://doi.org/10.1038/nrmicro.2016.94

Franks, A. E., Nevin, K. P., Jia, H., Izallalen, M., Woodard, T. L., & Lovley, D. R. (2009). Novel strategy for three-dimensional real-time imaging of microbial fuel cell communities: Monitoring the inhibitory effects of proton accumulation within the anode biofilm. *Energy Environ. Sci.*, *2*(1), 113–119. https://doi.org/10.1039/B816445B

Geng, Y., Wang, M., Sarkis, J., Xue, B., Zhang, L., Fujita, T., Yu, X., Ren, W., Zhang, L., & Dong, H. (2014). Spatial-temporal patterns and driving factors for industrial wastewater emission in China. *Journal of Cleaner Production*, *76*, 116–124. https://doi.org/10.1016/j.jclepro.2014.04.047

Gou, P., Kraut, N. D., Feigel, I. M., Bai, H., Morgan, G. J., Chen, Y., Tang, Y., Bocan, K., Stachel, J., Berger, L., Mickle, M., Sejdić, E., & Star, A. (2015). Carbon Nanotube Chemiresistor for Wireless pH Sensing. *Scientific Reports*, *4*(1), 4468. https://doi.org/10.1038/srep04468

Guimerà, X., Moya, A., Dorado, A. D., Illa, X., Villa, R., Gabriel, D., Gamisans, X., & Gabriel, G. (2019). A Minimally Invasive Microsensor Specially Designed for Simultaneous Dissolved Oxygen and pH Biofilm Profiling. *Sensors*, *19*(21), 4747. https://doi.org/10.3390/s19214747

Gul, O., Mortas, M., Atalar, I., Dervisoglu, M., & Kahyaoglu, T. (2015). Manufacture and characterization of kefir made from cow and buffalo milk, using kefir grain and starter culture. *Journal of Dairy Science*, *98*(3), 1517–1525. https://doi.org/10.3168/jds.2014-8755

Gümpel, P., Arlt, N., Telegdi, J., Schiller, D., & Moos, O. (2006). Microbiological influence on the electro-chemical potential of stainless steel. *Materials and Corrosion*, *57*(9), 715–723. https://doi.org/10.1002/maco.200503962

Hach. (2018). *Chlorine Sensor*.

Haile, M., & Kang, W. H. (2019). The Role of Microbes in Coffee Fermentation and Their Impact on Coffee Quality. *Journal of Food Quality*, *2019*, 1–6. https://doi.org/10.1155/2019/4836709

Hall, J. S., & Szabo, J. G. (2009). *Distribution System Water Quality Monitoring: Sensor Technology Evaluation Methodology and Results—A Guide for Sensor Manufacturers and Water Utilities*. *EPA 817-B-15-002*, 60.

Hall-Stoodley, L., Stoodley, P., Kathju, S., Høiby, N., Moser, C., William Costerton, J., Moter, A., & Bjarnsholt, T. (2012). Towards diagnostic guidelines for biofilm-associated infections. *FEMS Immunology & Medical Microbiology*, *65*(2), 127–145. https://doi.org/10.1111/j.1574-695X.2012.00968.x

He, X., Chadwick, G., Jiménez Otero, F., Orphan, V., & Meile, C. (2021). Spatially Resolved Electron Transport through Anode-Respiring *Geobacter sulfurreducens* Biofilms: Controls and Constraints. *ChemElectroChem*, *8*(10), 1747–1758. https://doi.org/10.1002/celc.202100111

Hinsinger, P., Plassard, C., & Jaillard, B. (2006). Rhizosphere: A new frontier for soil biogeochemistry. *Journal of Geochemical Exploration*, *88*(1–3), 210–213. https://doi.org/10.1016/j.gexplo.2005.08.041

Hols, P., Kleerebezem, M., Schanck, A. N., Ferain, T., Hugenholtz, J., Delcour, J., & de Vos, W. M. (1999). Conversion of Lactococcus lactis from homolactic to homoalanine fermentation through metabolic engineering. *Nature Biotechnology*, *17*(6), 588–592. https://doi.org/10.1038/9902

Holtmann, D., Schrader, J., & Sell, D. (2006). Quantitative Comparison of the Signals of an Electrochemical Bioactivity Sensor During the Cultivation of Different Microorganisms. *Biotechnology Letters*, *28*(12), 889–896. https://doi.org/10.1007/s10529-006-9021-y

Hristovski, K. D., Burge, S. R., Boscovic, D., Burge, R. G., & Babanovska-Milenkovska, F. (2022). Real-time monitoring of kefir-facilitated milk fermentation using microbial potentiometric sensors. *Journal of Environmental Chemical Engineering*, *10*(3), 107491. https://doi.org/10.1016/j.jece.2022.107491

Husson, O. (2013). Redox potential (Eh) and pH as drivers of soil/plant/microorganism systems: A transdisciplinary overview pointing to integrative opportunities for agronomy. *Plant and Soil*, *362*(1–2), 389–417. https://doi.org/10.1007/s11104-012-1429-7

Hyde, K. (2019). *Hyde 2019- Using passive anode-cathod technology to assess microbial happiness and boost benzene biodegredation rates.pdf*. Sustainable In-Situ Remediation Co-operative Alliance, University of Saskatchewan. https://esaa.org/wp-content/uploads/2021/04/19-Hyde.pdf

Jamal, M., Ahmad, W., Andleeb, S., Jalil, F., Imran, M., Nawaz, M. A., Hussain, T., Ali, M., Rafiq, M., & Kamil, M. A. (2018). Bacterial biofilm and associated infections. *Journal of the Chinese Medical Association*, *81*(1), 7–11. https://doi.org/10.1016/j.jcma.2017.07.012

Janknecht, P., & Melo, L. F. (2003). Online Biofilm Monitoring. *Reviews in Environmental Science and Bio/Technology*, *2*(2–4), 269–283. https://doi.org/10.1023/B:RESB.0000040461.69339.04

Jiang, C., Yao, Y., Cai, Y., & Ping, J. (2019). All-solid-state potentiometric sensor using single-walled carbon nanohorns as transducer. *Sensors and Actuators B: Chemical*, *283*, 284–289. https://doi.org/10.1016/j.snb.2018.12.040

Jiménez Otero, F., Chadwick, G. L., Yates, M. D., Mickol, R. L., Saunders, S. H., Glaven, S. M., Gralnick, J. A., Newman, D. K., Tender, L. M., Orphan, V. J., & Bond, D. R. (2021). Evidence of a Streamlined Extracellular Electron Transfer Pathway from Biofilm Structure, Metabolic Stratification, and Long-Range Electron Transfer Parameters. *Applied and Environmental Microbiology*, *87*(17). https://doi.org/10.1128/AEM.00706-21

Kang, J., Kim, T., Tak, Y., Lee, J.-H., & Yoon, J. (2012). Cyclic voltammetry for monitoring bacterial attachment and biofilm formation. *Journal of Industrial and Engineering Chemistry*, *18*(2), 800–807. https://doi.org/10.1016/j.jiec.2011.10.002

Kang, K. H., Jang, J. K., & Kim, H. (2003). *A microbial fuel cell with improved cathode reaction as a low biochemical oxygen demand sensor*. 5. https://doi.org/10.1023/a:1024984521699.

Kaplan, J. B. (2010). Biofilm Dispersal: Mechanisms, Clinical Implications, and Potential Therapeutic Uses. *Journal of Dental Research*, *89*(3), 205–218. https://doi.org/10.1177/0022034509359403

Kara, S., Keskinler, B., & Erhan, E. (2009). A novel microbial BOD biosensor developed by the immobilization of *P. Syringae* in micro-cellular polymers. *Journal of Chemical Technology & Biotechnology*, *84*(4), 511–518. https://doi.org/10.1002/jctb.2071

Khatoon, Z., McTiernan, C. D., Suuronen, E. J., Mah, T.-F., & Alarcon, E. I. (2018). Bacterial biofilm formation on implantable devices and approaches to its treatment and prevention. *Heliyon*, *4*(12), e01067. https://doi.org/10.1016/j.heliyon.2018.e01067

Kim, B. H., Chang, I. S., Gil, G. C., Park, H. S., & Kim, H. J. (2003). *Novel BOD (biological oxygen demand) sensor using mediator-less microbial fuel cell*. 5. https://doi-org.ezproxy1.lib.asu.edu/10.1023/A:1022891231369

Kumar, M., Gogoi, A., & Mukherjee, S. (2020). Metal removal, partitioning and phase distributions in the wastewater and sludge: Performance evaluation of conventional, upflow anaerobic sludge blanket and downflow hanging sponge treatment systems. *Journal of Cleaner Production*, *249*, 119426. https://doi.org/10.1016/j.jclepro.2019.119426

Lafitte, V. G. H., Wang, W., Yashina, A. S., & Lawrence, N. S. (2008). Anthraquinone–ferrocene film electrodes: Utility in pH and oxygen sensing. *Electrochemistry Communications*, *10*(12), 1831–1834. https://doi.org/10.1016/j.elecom.2008.09.031

Laureys, D., & De Vuyst, L. (2014). Microbial Species Diversity, Community Dynamics, and Metabolite Kinetics of Water Kefir Fermentation. *Applied and Environmental Microbiology*, *80*(8), 2564–2572. https://doi.org/10.1128/AEM.03978-13

Laureys, D., & De Vuyst, L. (2017). The water kefir grain inoculum determines the characteristics of the resulting water kefir fermentation process. *Journal of Applied Microbiology*, *122*(3), 719–732. https://doi.org/10.1111/jam.13370

LeChevallier, M. W., Lowry, C. D., & Lee, R. G. (1990). Disinfecting Biofilms in a Model Distribution System. *Journal - American Water Works Association*, *82*(7), 87–99. https://doi.org/10.1002/j.1551-8833.1990.tb06996.x

Lei, Y., Mulchandani, P., Chen, W., & Mulchandani, A. (2007). Biosensor for direct determination of fenitrothion and EPN using recombinant Pseudomonas putida JS444 with surface-expressed organophosphorous hydrolase. 2. Modified carbon paste electrode. *Applied Biochemistry and Biotechnology*, *136*(3), 243–250. https://doi.org/10.1007/s12010-007-9023-9

Lester, M. B., & van Riper III, C. (2014). *Distribution and Extent of Heavy Metal Accumulation in Song Sparrows (Melospiza melodia), Upper Santa Cruz River Watershed, Southern Arizona, 2011–12* (Open-File Report Open-File Report 2014–1072; Open-File Report). U.S. Department of the Interior U.S. Geological Survey. ISSN 2331-1258

Levar, C. E., Chan, C. H., Mehta-Kolte, M. G., & Bond, D. R. (2014). An Inner Membrane Cytochrome Required Only for Reduction of High Redox Potential Extracellular Electron Acceptors. *MBio*, *5*(6). https://doi.org/10.1128/mBio.02034-14

Lewandowski, Z., & Beyenal, H. (2013). Imaging and characterizing biofilm components. In *Fundamentals of Biofilm Research* (2nd ed.). CRC Press.

Li, D., Li, J., Liu, D., Ma, X., Cheng, L., Li, W., Qian, C., Mu, Y., & Yu, H. (2019). Potential regulates metabolism and extracellular respiration of electroactive *Geobacter* biofilm. *Biotechnology and Bioengineering*, *116*(5), 961–971. https://doi.org/10.1002/bit.26928

Liptzin, D., Silver, W. L., & Detto, M. (2011). Temporal Dynamics in Soil Oxygen and Greenhouse Gases in Two Humid Tropical Forests. *Ecosystems*, *14*(2), 171–182. https://doi.org/10.1007/s10021-010-9402-x

Liu, J., Prindle, A., Humphries, J., Gabalda-Sagarra, M., Asally, M., Lee, D. D., Ly, S., Garcia-Ojalvo, J., & Süel, G. M. (2015). Metabolic co-dependence gives rise to collective oscillations within biofilms. *Nature*, *523*(7562), 550–554. https://doi.org/10.1038/nature14660

Logan, B. E. (2009). Exoelectrogenic bacteria that power microbial fuel cells. *Nature Reviews Microbiology*, *7*(5), 375–381. https://doi.org/10.1038/nrmicro2113

Logan, B. E., Hamelers, B., Rozendal, R., Schröder, U., Keller, J., Freguia, S., Aelterman, P., Verstraete, W., & Rabaey, K. (2006). Microbial Fuel Cells: Methodology and Technology. *Environmental Science & Technology*, *40*(17), 5181–5192. https://doi.org/10.1021/es0605016

Logan, B. E., & Rabaey, K. (2012). Conversion of Wastes into Bioelectricity and Chemicals by Using Microbial Electrochemical Technologies. *Science*, *337*(6095), 686–690. https://doi.org/10.1126/science.1217412

Logan, B. E., & Regan, J. M. (2006a). *Harnessing the metabolic activity of bacteria can provide energy for a variety of applications, once technical and cost obstacles are overcome.* 9. https://doi-org.ezproxy1.lib.asu.edu/10.1021/es0627592

Logan, B. E., & Regan, J. M. (2006b). Electricity-producing bacterial communities in microbial fuel cells. *Trends in Microbiology*, *14*(12), 512–518. https://doi.org/10.1016/j.tim.2006.10.003

Lopez, D., Vlamakis, H., & Kolter, R. (2010). Biofilms. *Cold Spring Harbor Perspectives in Biology*, *2*(7), a000398–a000398. https://doi.org/10.1101/cshperspect.a000398

Luedeking, R., & Piret, E. (1959). Journal of Biochemical and Microbiological Technology and Engineering. *Nature*, *183*(4672), 1367–1367. https://doi.org/10.1038/1831367e0

Macià, M. D., del Pozo, J. L., Díez-Aguilar, M., & Guinea, J. (2018). Diagnóstico microbiológico de las infecciones relacionadas con la formación de biopelículas. *Enfermedades Infecciosas y Microbiología Clínica*, *36*(6), 375–381. https://doi.org/10.1016/j.eimc.2017.04.006

Magnuson, T. S., Isoyama, N., Hodges-Myerson, A. L., Davidson, G., Maroney, M. J., Geesey, G. G., & Lovley, D. R. (2001). *Isolation, characterization and gene sequence analysis of a membrane- associated 89 kDa Fe(III) reducing cytochrome c from*. 6.

Mansfeldt, T. (2003). *In situ* long-term redox potential measurements in a dyked marsh soil. *Journal of Plant Nutrition and Soil Science*, *166*(2), 210–219. https://doi.org/10.1002/jpln.200390031

Manuel, C. M., Nunes, O. C., & Melo, L. F. (2007). Dynamics of drinking water biofilm in flow/non-flow conditions. *Water Research*, *41*(3), 551–562. https://doi.org/10.1016/j.watres.2006.11.007

Mattila, M., Carpen, L., Hakkarainen, T., & Salkinoja-Salonen, M. S. (1997). Biofilm development during ennoblement of stainless steel in Baltic Sea water: A microscopic study. *International Biodeterioration & Biodegradation*, *40*(1), 1–10. https://doi.org/10.1016/S0964-8305(97)00003-6

Mattila-Sandholm, T., & Wirtanen, G. (1992). Biofilm formation in the industry: A review. *Food Reviews International*, *8*(4), 573–603. https://doi.org/10.1080/87559129209540953

McDougald, D., Rice, S. A., Barraud, N., Steinberg, P. D., & Kjelleberg, S. (2012). Should we stay or should we go: Mechanisms and ecological consequences for biofilm dispersal. *Nature Reviews Microbiology*, *10*(1), 39–50. https://doi.org/10.1038/nrmicro2695

Mermel, L. A. (2000). *Prevention of Intravascular Catheter–Related Infections*. 12.

Meyer, A. M., Klein, C., Fünfrocken, E., Kautenburger, R., & Beck, H. P. (2019). Real-time monitoring of water quality to identify pollution pathways in small and middle scale rivers. *Science of The Total Environment*, *651*, 2323–2333. https://doi.org/10.1016/j.scitotenv.2018.10.069

Monds, R. D., & O'Toole, G. A. (2009). The developmental model of microbial biofilms: Ten years of a paradigm up for review. *Trends in Microbiology*, *17*(2), 73–87. https://doi.org/10.1016/j.tim.2008.11.001

Moscoviz, R., Toledo-Alarcón, J., Trably, E., & Bernet, N. (2016). Electro-Fermentation: How To Drive Fermentation Using Electrochemical Systems. *Trends in Biotechnology*, *34*(11), 856–865. https://doi.org/10.1016/j.tibtech.2016.04.009

Mueller, T. G., Pierce, F. J., Schabenberger, O., & Warncke, D. D. (2001). Map Quality for Site-Specific Fertility Management. *Soil Science Society of America Journal*, *65*(5), 1547–1558. https://doi.org/10.2136/sssaj2001.6551547x

Mulchandani, P., Chen, W., & Mulchandani, A. (2006). Microbial biosensor for direct determination of nitrophenyl-substituted organophosphate nerve agents using genetically engineered Moraxella sp. *Analytica Chimica Acta*, *568*(1–2), 217–221. https://doi.org/10.1016/j.aca.2005.11.063

Myers, J. M., & Myers, C. R. (2001). Role for Outer Membrane Cytochromes OmcA and OmcB of *Shewanella putrefaciens* MR-1 in Reduction of Manganese Dioxide. *Applied and Environmental Microbiology*, *67*(1), 260–269. https://doi.org/10.1128/AEM.67.1.260-269.2001

Nguyen, B. T. T., Koh, G., Lim, H. S., Chua, A. J. S., Ng, M. M. L., & Toh, C.-S. (2009). Membrane-Based Electrochemical Nanobiosensor for the Detection of Virus. *Analytical Chemistry*, *81*(17), 7226–7234. https://doi.org/10.1021/ac900761a

Nguyen, T., Roddick, F., & Fan, L. (2012). Biofouling of Water Treatment Membranes: A Review of the Underlying Causes, Monitoring Techniques and Control Measures. *Membranes*, *2*(4), 804–840. https://doi.org/10.3390/membranes2040804

Nivens, D. E., Co, B. M., & Franklin, M. J. (2009). Sampling and quantification of biofilms in food processing and other environments. In *Biofilms in the Food and Beverage Industries* (pp. 539–568). Elsevier. https://doi.org/10.1533/9781845697167.5.539

Nivens, D. E., Palmer, R. J., & White, D. C. (1995). Continuous nondestructive monitoring of microbial biofilms: A review of analytical techniques. *Journal of Industrial Microbiology*, *15*(4), 263–276. https://doi.org/10.1007/BF01569979

Ntsame Affane, A. L., Fox, G. P., Sigge, G. O., Manley, M., & Britz, T. J. (2011). Simultaneous prediction of acidity parameters (pH and titratable acidity) in Kefir using near infrared reflectance spectroscopy. *International Dairy Journal*, *21*(11), 896–900. https://doi.org/10.1016/j.idairyj.2011.04.016

O'Mara, P., Farrell, A., Bones, J., & Twomey, K. (2018). Staying alive! Sensors used for monitoring cell health in bioreactors. *Talanta*, *176*, 130–139. https://doi.org/10.1016/j.talanta.2017.07.088

Pareek, N. K. (1992). Industrial Wastewater Management in Developing Countries. *Water Science and Technology*, *25*(1), 69–74. https://doi.org/10.2166/wst.1992.0011

Pereira, A., Pinho, J. L. S., Faria, R., Vieira, J. M. P., & Costa, C. (2019). Improving operational management of wastewater systems. A case study. *Water Science and Technology*, *80*(1), 173–183. https://doi.org/10.2166/wst.2019.264

Poma, N., Vivaldi, F., Bonini, A., Salvo, P., Kirchhain, A., Ates, Z., Melai, B., Bottai, D., Tavanti, A., & Di Francesco, F. (2021). Microbial biofilm monitoring by electrochemical transduction methods. *TrAC Trends in Analytical Chemistry*, *134*, 116134. https://doi.org/10.1016/j.trac.2020.116134

Poma, N., Vivaldi, F., Bonini, A., Salvo, P., Kirchhain, A., Melai, B., Bottai, D., Tavanti, A., & Di Francesco, F. (2020). A graphenic and potentiometric sensor for monitoring the growth of bacterial biofilms. *Sensors and Actuators B: Chemical*, *323*, 128662. https://doi.org/10.1016/j.snb.2020.128662

Prindle, A., Liu, J., Asally, M., Ly, S., Garcia-Ojalvo, J., & Süel, G. M. (2015). Ion channels enable electrical communication in bacterial communities. *Nature*, *527*(7576), 59–63. https://doi.org/10.1038/nature15709

Punter, J., Colomer-Farrarons, J., & Ll., P. (2013). Bioelectronics for Amperometric Biosensors. In T. Rinken (Ed.), *State of the Art in Biosensors—General Aspects*. InTech. https://doi.org/10.5772/52248

Qiu, J., Arnold, M. A., & Murhammer, D. W. (2014). On-line near infrared bioreactor monitoring of cell density and concentrations of glucose and lactate during insect cell cultivation. *Journal of Biotechnology*, *173*, 106–111. https://doi.org/10.1016/j.jbiotec.2014.01.009

Rabaey, K., Rodríguez, J., Blackall, L. L., Keller, J., Gross, P., Batstone, D., Verstraete, W., & Nealson, K. H. (2007). Microbial ecology meets electrochemistry: Electricity-driven and driving communities. *The ISME Journal*, *1*(1), 9–18. https://doi.org/10.1038/ismej.2007.4

Rabenhorst, M. C., Hively, W. D., & James, B. R. (2009). Measurements of Soil Redox Potential. *Soil Science Society of America Journal*, *73*(2), 668–674. https://doi.org/10.2136/sssaj2007.0443

Radzevič, A., Niaura, G., Ignatjev, I., Rakickas, T., Celiešiūtė, R., & Pauliukaite, R. (2016). Electropolymerisation of the natural monomer riboflavin and its characterisation. *Electrochimica Acta*, *222*, 1818–1830. https://doi.org/10.1016/j.electacta.2016.11.166

Ramos, J.-L., Valdivia, M., García-Lorente, F., & Segura, A. (2016). Benefits and perspectives on the use of biofuels. *Microbial Biotechnology*, *9*(4), 436–440. https://doi.org/10.1111/1751-7915.12356

Reguera, G., Nevin, K. P., Nicoll, J. S., Covalla, S. F., Woodard, T. L., & Lovley, D. R. (2006). Biofilm and Nanowire Production Leads to Increased Current in *Geobacter sulfurreducens* Fuel Cells. *Applied and Environmental Microbiology*, *72*(11), 7345–7348. https://doi.org/10.1128/AEM.01444-06

Reinecke, T., Biechele, P., Sobocinski, M., Suhr, H., Bakes, K., Solle, D., Jantunen, H., Scheper, T., & Zimmermann, S. (2017). Continuous noninvasive monitoring of cell growth in disposable bioreactors. *Sensors and Actuators B: Chemical*, *251*, 1009–1017. https://doi.org/10.1016/j.snb.2017.05.111

Rice, D., Westerhoff, P., Perreault, F., & Garcia-Segura, S. (2018). Electrochemical self-cleaning anodic surfaces for biofouling control during water treatment.

Electrochemistry Communications, *96*, 83–87. https://doi.org/10.1016/j.elecom.2018.10.002

Rimboud, M., Desmond-Le Quemener, E., Erable, B., Bouchez, T., & Bergel, A. (2015). Multi-system Nernst–Michaelis–Menten model applied to bioanodes formed from sewage sludge. *Bioresource Technology*, *195*, 162–169. https://doi.org/10.1016/j.biortech.2015.05.069

Rosa, D. D., Dias, M. M. S., Grześkowiak, Ł. M., Reis, S. A., Conceição, L. L., & Peluzio, M. do C. G. (2017). Milk *kefir*: Nutritional, microbiological and health benefits. *Nutrition Research Reviews*, *30*(1), 82–96. https://doi.org/10.1017/S0954422416000275

Saboe, D., Ghasemi, H., Gao, M. M., Samardzic, M., Hristovski, K. D., Boscovic, D., Burge, S. R., Burge, R. G., & Hoffman, D. A. (2021). Real-time monitoring and prediction of water quality parameters and algae concentrations using microbial potentiometric sensor signals and machine learning tools. *Science of The Total Environment*, *764*, 142876. https://doi.org/10.1016/j.scitotenv.2020.142876

Saboe, D., Hristovski, K. D., Burge, S. R., Burge, R. G., Taylor, E., & Hoffman, D. A. (2021). Measurement of free chlorine levels in water using potentiometric responses of biofilms and applications for monitoring and managing the quality of potable water. *Science of The Total Environment*, *766*, 144424. https://doi.org/10.1016/j.scitotenv.2020.144424

Sak, H., Senior, A., & Beaufays, F. (2014). Long Short-Term Memory Based Recurrent Neural Network Architectures for Large Vocabulary Speech Recognition. *ArXiv:1402.1128 [Cs, Stat]*. http://arxiv.org/abs/1402.1128

Salvo, P., Calisi, N., Melai, B., Cortigiani, B., Mannini, M., Caneschi, A., Lorenzetti, G., Paoletti, C., Lomonaco, T., Paolicchi, A., Scataglini, I., Dini, V., Romanelli, M., Fuoco, R., & Di Francesco, F. (2017). Temperature and pH sensors based on graphenic materials. *Biosensors and Bioelectronics*, *91*, 870–877. https://doi.org/10.1016/j.bios.2017.01.062

Satir, G., & Guzel-Seydim, Z. B. (2016). How kefir fermentation can affect product composition? *Small Ruminant Research*, *134*, 1–7. https://doi.org/10.1016/j.smallrumres.2015.10.022

Schievano, A., Pepé Sciarria, T., Vanbroekhoven, K., De Wever, H., Puig, S., Andersen, S. J., Rabaey, K., & Pant, D. (2016). Electro-Fermentation – Merging Electrochemistry with Fermentation in Industrial Applications. *Trends in Biotechnology*, *34*(11), 866–878. https://doi.org/10.1016/j.tibtech.2016.04.007

Scholz, F. (2015). Voltammetric techniques of analysis: The essentials. *ChemTexts*, *1*(4), 17. https://doi.org/10.1007/s40828-015-0016-y

Schröder, U. (2007). Anodic electron transfer mechanisms in microbial fuel cells and their energy efficiency. *Phys. Chem. Chem. Phys.*, *9*(21), 2619–2629. https://doi.org/10.1039/B703627M

Schrott, G. D., Bonanni, P. S., Robuschi, L., Esteve-Nuñez, A., & Busalmen, J. P. (2011). Electrochemical insight into the mechanism of electron transport in biofilms of Geobacter sulfurreducens. *Electrochimica Acta*, *56*(28), 10791–10795. https://doi.org/10.1016/j.electacta.2011.07.001

Sensorx. (2011). *Free Chlorine Amperometric 4-20mA Sensors*.

Shao, Y., Ying, Y., & Ping, J. (2020). Recent advances in solid-contact ion-selective electrodes: Functional materials, transduction mechanisms, and development trends. *Chemical Society Reviews*, *49*(13), 4405–4465. https://doi.org/10.1039/C9CS00587K

Shi, L., Squier, T. C., Zachara, J. M., & Fredrickson, J. K. (2007). Respiration of metal (hydr)oxides by *Shewanella* and *Geobacter*: A key role for multihaem *c* -type cytochromes. *Molecular Microbiology*, *65*(1), 12–20. https://doi.org/10.1111/j.1365-2958.2007.05783.x

Si, R.-W., Yang, Y., Yu, Y.-Y., Han, S., Zhang, C.-L., Sun, D.-Z., Zhai, D.-D., Liu, X., & Yong, Y.-C. (2016). Wiring Bacterial Electron Flow for Sensitive Whole-Cell Amperometric Detection of Riboflavin. *Analytical Chemistry*, *88*(22), 11222–11228. https://doi.org/10.1021/acs.analchem.6b03538

Singh, M., Nesakumar, N., Sethuraman, S., Krishnan, U. M., & Rayappan, J. B. B. (2014). Electrochemical biosensor with ceria–polyaniline core shell nano-interface for the detection of carbonic acid in blood. *Journal of Colloid and Interface Science*, *425*, 52–58. https://doi.org/10.1016/j.jcis.2014.03.041

Snider, R. M., Strycharz-Glaven, S. M., Tsoi, S. D., Erickson, J. S., & Tender, L. M. (2012). Long-range electron transport in *Geobacter sulfurreducens* biofilms is redox gradient-driven. *Proceedings of the National Academy of Sciences*, *109*(38), 15467–15472. https://doi.org/10.1073/pnas.1209829109

Sophocleous, M., & Atkinson, J. K. (2017). A review of screen-printed silver/silver chloride (Ag/AgCl) reference electrodes potentially suitable for environmental potentiometric sensors. *Sensors and Actuators A: Physical*, *267*, 106–120. https://doi.org/10.1016/j.sna.2017.10.013

Spellman, F. R. (2003). *Handbook of water and wastewater treatment plant operations*. Lewis Publishers.

Stewart, P. S., & Franklin, M. J. (2008). Physiological heterogeneity in biofilms. *Nature Reviews Microbiology*, *6*(3), 199–210. https://doi.org/10.1038/nrmicro1838

Stoianov, I., Nachman, L., Whittle, A., Madden, S., & Kling, R. (2008). Sensor Networks for Monitoring Water Supply and Sewer Systems: Lessons from Boston. *Water Distribution Systems Analysis Symposium 2006*, 1–17. https://doi.org/10.1061/40941(247)100

Strathmann, M., Mittenzwey, K.-H., Sinn, G., Papadakis, W., & Flemming, H.-C. (2013). Simultaneous monitoring of biofilm growth, microbial activity, and inorganic deposits on surfaces with an *in situ* , online, real-time, non-destructive, optical sensor. *Biofouling*, *29*(5), 573–583. https://doi.org/10.1080/08927014.2013.791287

Streeter, I., Leventis, HenryC., Wildgoose, GregoryG., Pandurangappa, M., Lawrence, NathanS., Jiang, L., Jones, TimothyG. J., & Compton, RichardG. (2004). A sensitive reagentless pH probe with a ca. 120 mV/pH unit response. *Journal of Solid State Electrochemistry*, *8*(10). https://doi.org/10.1007/s10008-004-0536-7

Surman, S. B., Walker, J. T., Goddard, D. T., Morton, L. H. G., Keevil, C. W., Weaver, W., Skinner, A., Hanson, K., Caldwell, D., & Kurtz, J. (1996). Comparison of microscope techniques for the examination of biofilms. *Journal of Microbiological Methods*, *25*(1), 57–70. https://doi.org/10.1016/0167-7012(95)00085-2

Syafrudin, M., Alfian, G., Fitriyani, N., & Rhee, J. (2018). Performance Analysis of IoT-Based Sensor, Big Data Processing, and Machine Learning Model for Real-Time Monitoring System in Automotive Manufacturing. *Sensors*, *18*(9), 2946. https://doi.org/10.3390/s18092946

Sydow, A., Krieg, T., Mayer, F., Schrader, J., & Holtmann, D. (2014). Electroactive bacteria—Molecular mechanisms and genetic tools. *Applied Microbiology and Biotechnology*, *98*(20), 8481–8495. https://doi.org/10.1007/s00253-014-6005-z

Tang, J., Hinds, S., Kelley, S. O., & Sargent, E. H. (2008). Synthesis of Colloidal $CuGaSe_2$, $CuInSe_2$, and $Cu(InGa)Se_2$ Nanoparticles. *Chemistry of Materials*, *20*(22), 6906–6910. https://doi.org/10.1021/cm801655w

Telegdi, J., Shaban, A., & Trif, L. (2017). Microbiologically influenced corrosion (MIC). In *Trends in Oil and Gas Corrosion Research and Technologies* (pp. 191–214). Elsevier. https://doi.org/10.1016/B978-0-08-101105-8.00008-5

Thabane, L., Ma, J., Chu, R., Cheng, J., Ismaila, A., Rios, L. P., Robson, R., Thabane, M., Giangregorio, L., & Goldsmith, C. H. (2010). A tutorial on pilot studies: The what, why and how. *BMC Medical Research Methodology*, *10*(1), 1. https://doi.org/10.1186/1471-2288-10-1

Thabane, L., Mbuagbaw, L., Zhang, S., Samaan, Z., Marcucci, M., Ye, C., Thabane, M., Giangregorio, L., Dennis, B., Kosa, D., Debono, V. B., Dillenburg, R., Fruci, V., Bawor, M., Lee, J., Wells, G., & Goldsmith, C. H. (2013). A tutorial on sensitivity analyses in clinical trials: The what, why, when and how. *BMC Medical Research Methodology*, *13*(1), 92. https://doi.org/10.1186/1471-2288-13-92

Thet, N. T., Alves, D. R., Bean, J. E., Booth, S., Nzakizwanayo, J., Young, A. E. R., Jones, B. V., & Jenkins, A. T. A. (2016). Prototype Development of the Intelligent Hydrogel Wound Dressing and Its Efficacy in the Detection of Model Pathogenic Wound Biofilms. *ACS Applied Materials & Interfaces*, *8*(24), 14909–14919. https://doi.org/10.1021/acsami.5b07372

Thomen, P., Robert, J., Monmeyran, A., Bitbol, A.-F., Douarche, C., & Henry, N. (2017). Bacterial biofilm under flow: First a physical struggle to stay, then a matter of breathing. *PLOS ONE*, *12*(4), e0175197. https://doi.org/10.1371/journal.pone.0175197

Torres, C. I., Kato Marcus, A., & Rittmann, B. E. (2008). Proton transport inside the biofilm limits electrical current generation by anode-respiring bacteria. *Biotechnology and Bioengineering*, *100*(5), 872–881. https://doi.org/10.1002/bit.21821

Trussell, R. S., Merlo, R. P., Hermanowicz, S. W., & Jenkins, D. (2007). Influence of mixed liquor properties and aeration intensity on membrane fouling in a submerged membrane bioreactor at high mixed liquor suspended solids concentrations. *Water Research*, *41*(5), 947–958. https://doi.org/10.1016/j.watres.2006.11.012

U.S. EPA. (n.d.). Water Quality Surveillance and Response System Primer. *United States Environmental Protection Agency*, *EPA 817-B-15-002*, 14.

U.S. EPA, Office of Water. (1999). *25 Years of the Safe Drinking Water Act: History and Trends* (EPA 816-R-99-007).

U.S. EPA, Office of Water. (2016). *Definition and Procedure for the Determination of the Method Detection Limit, Revision 2*. U.S. EPA.

Vertes, A., Hitchins, V., & Phillips, K. S. (2012). Analytical Challenges of Microbial Biofilms on Medical Devices. *Analytical Chemistry*, *84*(9), 3858–3866. https://doi.org/10.1021/ac2029997

Vivaldi, F., Santalucia, D., Poma, N., Bonini, A., Salvo, P., Del Noce, L., Melai, B., Kirchhain, A., Kolivoška, V., Sokolová, R., Hromadová, M., & Di Francesco, F. (2020). A voltammetric pH sensor for food and biological matrices. *Sensors and Actuators B: Chemical*, *322*, 128650. https://doi.org/10.1016/j.snb.2020.128650

Vonau, W., Oelßner, W., Guth, U., & Henze, J. (2010). An all-solid-state reference electrode. *Sensors and Actuators B: Chemical*, *144*(2), 368–373. https://doi.org/10.1016/j.snb.2008.12.001

Wang, 1948-, Joseph. (2006). Practical Considerations. In *Analytical electrochemistry /* (3rd ed.). Wiley-VCH,.

Wang, S.-L., Xu, X.-R., Sun, Y.-X., Liu, J.-L., & Li, H.-B. (2013). Heavy metal pollution in coastal areas of South China: A review. *Marine Pollution Bulletin*, *76*(1–2), 7–15. https://doi.org/10.1016/j.marpolbul.2013.08.025

Wang, Z., Cao, X., Liu, D., Hao, S., Du, G., Asiri, A. M., & Sun, X. (2016). Ternary NiCoP nanosheet array on a Ti mesh: A high-performance electrochemical sensor for glucose detection. *Chemical Communications*, *52*(100), 14438–14441. https://doi.org/10.1039/C6CC08078B

Wanzek, T., Keiluweit, M., Baham, J., Dragila, M. I., Fendorf, S., Fiedler, S., Nico, P. S., & Kleber, M. (2018). Quantifying biogeochemical heterogeneity in soil systems. *Geoderma*, *324*, 89–97. https://doi.org/10.1016/j.geoderma.2018.03.003

Weaver, W. M., Milisavljevic, V., Miller, J. F., & Di Carlo, D. (2012). Fluid Flow Induces Biofilm Formation in Staphylococcus epidermidis Polysaccharide Intracellular Adhesin-Positive Clinical Isolates. *Applied and Environmental Microbiology*, *78*(16), 5890–5896. https://doi.org/10.1128/AEM.01139-12

Whisler, F. D., Lance, J. C., & Linebarger, R. S. (1974). Redox Potentials in Soil Columns Intermittently Flooded With Sewage Water. *Journal of Environmental Quality*, *3*(1), 68–74. https://doi.org/10.2134/jeq1974.00472425000300010019x

Wi, Y. M., & Patel, R. (2018). Understanding Biofilms and Novel Approaches to the Diagnosis, Prevention, and Treatment of Medical Device-Associated Infections. *Infectious Disease Clinics of North America*, *32*(4), 915–929. https://doi.org/10.1016/j.idc.2018.06.009

Wilson, R. E., Stoianov, I., & O'Hare, D. (2019). Continuous Chlorine Detection in Drinking Water and a Review of New Detection Methods. *Johnson Matthey Technology Review*, *63*(2), 103–118. https://doi.org/10.1595/205651318X15367593796080

Winquist, F., Krantz-Rülcker, C., Wide, P., & Lundström, I. (1998). Monitoring of freshness of milk by an electronic tongue on the basis of voltammetry. *Measurement Science and Technology*, *9*(12), 1937–1946. https://doi.org/10.1088/0957-0233/9/12/002

Wiranto, G., Maulana, Y. Y., Hermida, I. D. P., Syamsu, I., & Mahmudin, D. (2015). Integrated online water quality monitoring. *2015 International Conference on Smart Sensors and Application (ICSSA)*, 111–115. https://doi.org/10.1109/ICSSA.2015.7322521

Wu, H., Moser, C., Wang, H.-Z., Høiby, N., & Song, Z.-J. (2015). Strategies for combating bacterial biofilm infections. *International Journal of Oral Science*, *7*(1), 1–7. https://doi.org/10.1038/ijos.2014.65

Xie, F., Cao, X., Qu, F., Asiri, A. M., & Sun, X. (2018). Cobalt nitride nanowire array as an efficient electrochemical sensor for glucose and H2O2 detection. *Sensors and Actuators B: Chemical*, *255*, 1254–1261. https://doi.org/10.1016/j.snb.2017.08.098

Xie, F., Liu, T., Xie, L., Sun, X., & Luo, Y. (2018). Metallic nickel nitride nanosheet: An efficient catalyst electrode for sensitive and selective non-enzymatic glucose sensing. *Sensors and Actuators B: Chemical*, *255*, 2794–2799. https://doi.org/10.1016/j.snb.2017.09.095

Xie, L., Asiri, A. M., & Sun, X. (2017). Monolithically integrated copper phosphide nanowire: An efficient electrocatalyst for sensitive and selective nonenzymatic glucose detection. *Sensors and Actuators B: Chemical*, *244*, 11–16. https://doi.org/10.1016/j.snb.2016.12.093

Xu, F., Duan, J., & Hou, B. (2010). Electron transfer process from marine biofilms to graphite electrodes in seawater. *Bioelectrochemistry*, *78*(1), 92–95. https://doi.org/10.1016/j.bioelechem.2009.09.010

Yang, J., Kwak, T. J., Zhang, X., McClain, R., Chang, W.-J., & Gunasekaran, S. (2016). Digital pH Test Strips for In-Field pH Monitoring Using Iridium Oxide-Reduced Graphene Oxide Hybrid Thin Films. *ACS Sensors*, *1*(10), 1235–1243. https://doi.org/10.1021/acssensors.6b00385

Yang, Y., Wu, Y., Hu, Y., Cao, Y., Poh, C. L., Cao, B., & Song, H. (2015). Engineering Electrode-Attached Microbial Consortia for High-Performance Xylose-Fed Microbial Fuel Cell. *ACS Catalysis*, *5*(11), 6937–6945. https://doi.org/10.1021/acscatal.5b01733

Yates, M. D., Eddie, B. J., Lebedev, N., Kotloski, N. J., Strycharz-Glaven, S. M., & Tender, L. M. (2018). On the relationship between long-distance and heterogeneous electron transfer in electrode-grown Geobacter sulfurreducens biofilms. *Bioelectrochemistry*, *119*, 111–118. https://doi.org/10.1016/j.bioelechem.2017.09.007

Yoho, R. A., Popat, S. C., Rago, L., Guisasola, A., & Torres, C. I. (2015). Anode Biofilms of *Geoalkalibacter ferrihydriticus* Exhibit Electrochemical Signatures of Multiple Electron Transport Pathways. *Langmuir*, *31*(45), 12552–12559. https://doi.org/10.1021/acs.langmuir.5b02953

Yoho, R. A., Popat, S. C., & Torres, C. I. (2014). Dynamic Potential-Dependent Electron Transport Pathway Shifts in Anode Biofilms of *Geobacter sulfurreducens*. *ChemSusChem*, *7*(12), 3413–3419. https://doi.org/10.1002/cssc.201402589

Yoo, H., Lee, D. J., Cho, D., Park, J., Nam, K. W., Cho, Y. T., Park, J. Y., Chen, X., & Hong, S. (2016). Magnetically-refreshable receptor platform structures for reusable nano-biosensor chips. *Nanotechnology*, *27*(4), 045502. https://doi.org/10.1088/0957-4484/27/4/045502

Yu, Y.-Y., Wang, J.-X., Si, R.-W., Yang, Y., Zhang, C.-L., & Yong, Y.-C. (2017). Sensitive amperometric detection of riboflavin with a whole-cell electrochemical sensor. *Analytica Chimica Acta*, *985*, 148–154. https://doi.org/10.1016/j.aca.2017.06.053

Zacharoff, L., Chan, C. H., & Bond, D. R. (2016). Reduction of low potential electron acceptors requires the CbcL inner membrane cytochrome of Geobacter sulfurreducens. *Bioelectrochemistry*, *107*, 7–13. https://doi.org/10.1016/j.bioelechem.2015.08.003

Zeng, X.-Y., Li, S.-W., Leng, Y., & Kang, X.-H. (2020). Structural and functional responses of bacterial and fungal communities to multiple heavy metal exposure in arid loess. *Science of The Total Environment*, *723*, 138081. https://doi.org/10.1016/j.scitotenv.2020.138081

APPENDIX A

LITERATURE REVIEW METHOD

A systematic literature review was commenced. Sixteen primary publications were reviewed, comprised entirely of peer-reviewed articles. Publications to review then were identified from citation database searches and obtained directly from publishers or through the Arizona State University Library's Interlibrary Library Loan system. Search criteria included ("microbial potentiometric" OR "potentiometric sensor" OR "microbial potentiometric sensor" OR "microbial sensor" OR "electrical potential" OR "potentiometric"), AND ("biofilm" OR "milk" OR "yogurt" OR "water" OR "soil"). Literature focusing on the health aspect of biofilms and including clinical trials were excluded if not supportive of background information, importance, or methodology. Duplicate results were removed. The systematic search frequently returned cross-referenced conference proceedings, book chapters, review articles, and peer-reviewed papers, which were then included for further review.

Following this collection, the obtained items were screened using the available title and abstract. Literature relevant to electrical potential, biofilm, health and safety, data analysis, and fermentation were then selected for full review. This literature review search resulted in a total of 206 items included that would inform this research in some capacity. While much of the literature was concerned with technology similar to MPS, including voltametric, potentiometric, and amperometric sensing methods, these studies would inform the previous development, challenges, and potential applications of this research. A select few papers investigate monitoring milk in some capacity, yet none have directly applied MPS as a method of monitoring the culturing of yogurt. Regardless, previous research documenting the development and importance of using monitoring

technologies in a variety of biochemical processes, including food and fermentation, assist this research and its methodology.